INTERNATIONAL JOURNAL OF CLIMATOLOGY
Int. J. Climatol. (2016)
Published online in Wiley Online Library
(wileyonlinelibrary.com) DOI: 10.1002/joc.4700

RMetS
Royal Meteorological Society

Teleconnections and analysis of long-term wind speed variability in the UAE

Mussie Seyoum Naizghi[a]* and Taha B. M. J. Ouarda[a,b]
[a] *Institute Center for Water and Environment (iWATER), Masdar Institute of Science and Technology, Abu Dhabi, UAE*
[b] *INRS-ETE, National Institute of Scientific Research, Quebec, Canada*

ABSTRACT: Wind energy accounts for a small share of the global energy consumption in spite of its widespread availability. One of the obstacles hindering exploitation of wind energy is the lack of proper wind speed assessment models. The wind energy field credibility has occasionally suffered from wind power potential estimation studies that were conducted based on very short wind speed records and which did not give consideration to inter-annual wind variability. The objective of this paper is to examine the long-term variability of wind speed in the United Arab Emirates (UAE) and its teleconnections with various global climate indices by using wind speed collected from six ground stations and a reanalysis dataset. Linear correlation analysis and wavelet analysis were used to characterize the interaction. The modified Mann–Kendall test and linear regression indicated that half of the stations show a significant wind speed trend at the 5% level. The cumulative sum and Bayesian change detection methods indicated that five of the stations present change points. Continuous wavelet transform of wind speed showed biannual periodicity in some stations, in addition to the annual one. Wavelet coherence analysis demonstrated that wind speed in the UAE is mainly associated with the North Atlantic Oscillation, East Atlantic Oscillation, El Niño Southern Oscillation and the Indian Ocean Dipole indices. The first two indices simultaneously modulate wind speed in the summer while the last two influence winter and autumn wind speeds. Step-wise multiple linear regression models were developed to select appropriate predictors among the various climate indices.

KEY WORDS teleconnections; wind speed variability; wavelet analysis; climate index; trend; climate index; trend; change point; UAE

Received 16 July 2015; Revised 24 December 2015; Accepted 29 January 2016

1. Introduction

Modern renewable energy sources contributed a tiny 9.7% of the overall global energy consumption in 2011. Nevertheless, the global penetration of wind power is expanding and the installed capacity has been increasing exponentially during the last two decades reaching 318 gigawatt (GW) in 2013 from barely 10.2 GW in 1998 – more than 30-fold increase in just 15 years (Fried, 2014). The rapid progress in wind power installation is expected to continue in the foreseeable future. By 2017, the global installed capacity of wind power is estimated to reach about 536.1 GW. Compared with the 10,000 GW global potential of wind power, the installed capacity will still be only about 5% by 2017 (Joselin Herbert *et al.*, 2007).

One reason for the low penetration of wind power is the lack of appropriate wind speed assessment efforts. Wind energy potential assessment effort that rely on very short wind speed records do not take into consideration the information concerning the inherent inter-annual variability in wind characteristics. These assessment efforts occasionally lead to projects that do not deliver the expected outputs once completed.

Specifically, the United Arab Emirates (UAE) has limited studies on wind energy and hence the nature of wind speed variability in the country and the factors that influence it are largely unknown. The objectives of this paper are to: (i) examine variability and change in wind speed time series by studying the presence of periodicity, trend and change points in the series; (ii) identify the teleconnections between wind speed in the UAE and climate oscillations by applying cross wavelet transform and wavelet coherence analysis; and (iii) develop multiple linear regression models to represent wind speed as a function of various climate indices.

The paper is organized as follows: Section 2 investigates relevant literature with particular attention to the region of study. Section 3 describes the region of study and the various datasets being used. The research methodology and the mathematical approach are outlined in Section 4. Section 5 presents the results and discusses the important findings of the research. Finally, conclusions are presented in Section 6.

2. Review of teleconnection studies

Recurring and persistent, large-scale patterns of climate anomalies that span over vast geographical areas are commonly termed ‘teleconnection patterns’ or simply

* Correspondence to: M. S. Naizghi, Institute Center for Water and Environment (iWATER), Masdar Institute of Science and Technology, P.O. Box 54224, Abu Dhabi, UAE. E-mail: mussiesn@gmail.com

'teleconnections'. The term teleconnection started to appear in the literature since 1935. However, its application and much of the work has been carried out since the 1960s (Diaz *et al.*, 2001).

Teleconnections link the fluctuations in the dynamic circulation of climate indices in one region to changes in climatological variables in another remote location. These dynamic circulations include the likes of the El Niño Southern Oscillation (ENSO) and the North Atlantic Oscillation (NAO). It has been demonstrated that wind speed and direction are affected by large-scale climate oscillations. For instance, European and North American wind speeds are affected by the annual variation of NAO (Kirchner-Bossi *et al.*, 2014; Scaife *et al.*, 2014; Smith *et al.*, 2014).

Teleconnections between inter-annual variations in tropical sea surface temperature and variations in hydro-climate have also been established by a number of studies in different parts of the world, for example in South America (Diaz *et al.*, 1998; Romero *et al.*, 2007), North America (Ropelewski and Halpert, 1986; Nasri *et al.*, 2013), Europe (Trigo *et al.*, 2004), Africa (Lee *et al.*, 2013; Ouachani *et al.*, 2013), Asia (Zhang *et al.*, 2007; Li *et al.*, 2008) and on global scale (Kiladis and Diaz, 1989). These studies explained how climate phenomena such as rainfall and temperature are coupled to sea surface temperature and pressure anomalies in some remote areas.

Some studies developed statistical methodologies that effectively modelled the impact of climate indices on hydro-climatic variables. El Adlouni *et al.* (2007) and Ouarda and El-Adlouni (2011) investigated and modelled the impact of Pacific Decadal Oscillation (PDO) on precipitations in the Southern USA whereas Lee *et al.* (2013) showed the impact of PDO and NAO on streamflows in locations in Africa. Using long-term patterns of climatic indices and the Empirical Mode Decomposition (EMD) procedure, Lee and Ouarda (2010) modelled the future evolution of extreme streamflows in Quebec, Canada.

A number of publications focused on the teleconnections between major climate indices and hydro-climatic phenomena in the Middle East. Cullen *et al.* (2002) examined the connection between the NAO index and Middle Eastern streamflows and asserted that streamflow variability in winter is affected by changes in the index. Tabari *et al.* (2014) investigated the link between the Arctic Oscillation (AO) fluctuations and the inter-annual variability of evapotranspiration in Iran and observed significant correlation between the two. Nazemosadat and Cordery (2000) revealed significant negative correlation between summer ENSO and autumn precipitation in the northern part of Iran. In Ghasemi and Khalili (2006) study, the association between AO and winter temperature in the same country was examined. Positive winter temperature anomalies were found to be caused by the negative phases of AO in the previous summer. Conversely, cooler temperatures were observed during the positive phases. Ouachani *et al.* (2013) explored the influence of ENSO, PDO and Mediterranean Oscillation Index (MOI) on the Southern Mediterranean precipitation and streamflow. A strong correlation between the indices and precipitation was reported.

A relatively limited number of publications dealt with teleconnections in the Arabian Peninsula. Charabi and Abdul-Wahab (2009) studied the effect of both ENSO and Indian Oscillation Dipole (IOD) on the rainfall in Oman and observed that rainfall events with extremely low or high magnitudes were positively associated with large amplitude of the indices. Rainfall anomalies in Kuwait were investigated and showed significant positive correlation with ENSO (Marcella and Eltahir, 2008). It, however, did not show significant correlation with NAO. Nasrallah *et al.* (2001) developed a statistical forecasting model for Kuwait winter precipitation by using climate indices, which include ENSO, Western Pacific (WP) and Northern Pacific (NP) among others, and was able to explain 70% of the precipitation variance which showed significant positive and negative correlation with ENSO and WP, respectively. A teleconnection study conducted on the southeastern region of the peninsula demonstrated that higher rainfall in Salalah is associated with El Niño conditions, while high rainfall in Muscat and Sharjah is associated with La Niña conditions (Brook and Sheen, 2000).

In the UAE, a few studies explored the teleconnections of the hydro-climate of the country with global climate oscillations. Ouarda *et al.* (2014) observed an overall decreasing precipitation trends in the UAE and identified a change point in the precipitation time series data around 1999 which was associated with the change of phase in the Southern Oscillation Index (SOI). In Niranjan Kumar and Ouarda (2014) study, the connections of ENSO and NAO with the precipitation variability in the UAE and the neighbouring regions were analyzed and found significant positive correlation between the rainfall and ENSO in contrast to limited negative correlation with NAO. The work also explained the physical mechanism governing the interaction between ENSO and precipitation variability. A more in-depth study of the remote influences of various climate oscillations on the temperature and precipitation in the UAE using linear correlation and wavelet analysis was conducted by Chandran *et al.* (2015). The work indicated that precipitation variability is associated with the SOI, PDO and IOD while the temperature variability is related to NAO, East Atlantic Oscillation (EAO) and Atlantic Multidecadal Oscillation (AMO).

In spite of the various studies on teleconnections of hydro-climatological variables with climate indices carried out in this region, very few studies have been carried out to explore the teleconnections of wind speed with the climate indices and none of them used wavelet techniques. All these studies were mainly carried out on temperature and precipitation data (Almazroui, 2012; Donat *et al.*, 2014). To the knowledge of the authors, this work represents a first effort to use continuous wavelet transform (CWT) to study wind speed data, and cross wavelet transform and wavelet coherence analysis to study wind speed teleconnections to climate circulation.

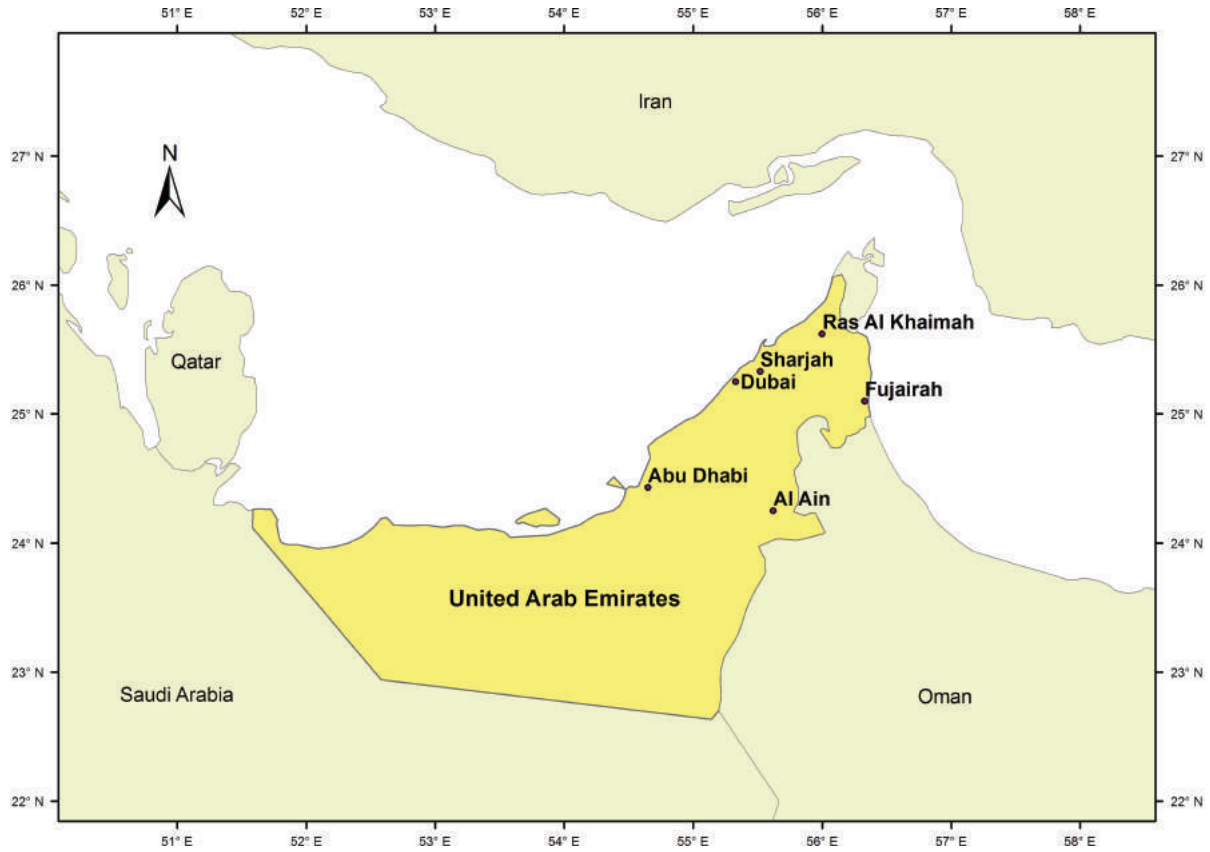

Figure 1. Geographical location of the ground stations.

3. Dataset description

Three sets of data were used in this work. The first set contains wind speed data from six ground stations. The second set consists of reanalysis data of wind speed in the UAE and surrounding regions. The last set comprises climate indices data.

3.1. Region of study and ground station data

The UAE is located in the southeastern end of the Arabian Peninsula along the Arabian Gulf between latitudes 22.5° and 26.5°N and longitudes 51.5° and 56.5°E (Figure 1) and covers a total area of 83,600 km^2. It is bordered by Oman in the east, Saudi Arabia in the west and the Arabian Gulf in the north. The country has an arid tropical climate with lowest annual rainfall of 63 mm in Abu Dhabi and highest of 127 mm in Ras Al Khaimah (Ouarda *et al.*, 2014). A limited number of studies targeting the wind regime of the country have been done. Ouarda *et al.* (2015) studied the probability density functions (pdf) of wind speed based on 10 min wind data collected from nine stations and identified the Kappa and Generalized Gamma distributions as the best one-parameter pdf's, Weibull distribution to be the best two-parameter pdf and mixture distributions in case of bimodal wind regimes. Furthermore, only a few studies dealt with the modelling of the UAE climate. Basha *et al.* (2015) developed long-term forecasts of climate variables in the UAE and predicted an increase in temperature and a decrease in rainfall in the next 30 years.

Six ground stations (Figure 1) located at the international airports of six cities of the UAE are considered in this study. The average daily wind speed, which is calculated by taking the average of the wind speed intensity (magnitude), in each station is obtained from the National Climatic Data Centre (NCDC) (http://www.ncdc.noaa.gov/). Of the six stations five are located in the coastal areas of both the Arabian Gulf (Abu Dhabi, Dubai, Sharjah and Ras Al Khaimah) and the Gulf of Oman (Fujairah). Al Ain station is located deep inland. Observational data is severely limited in the southern and southwestern parts of the country due to the lack of ground stations. The geographical coordinates, elevation, period of recording and summary of statistical characteristics of the stations are presented in Table 1.

3.2. Gridded NCEP/NCAR reanalysis data

The National Centre for Environmental Prediction (NCEP) and the National Centre for Atmospheric Research (NCAR) began 'The NCEP/NCAR Reanalysis Data' project in 1991 to provide accurate and global datasets on different atmospheric parameters (Kalnay *et al.*, 1996). The datasets incorporate numerical weather prediction model outputs and observed climate data originating from different metrological centres of individual countries. The archived reanalysis wind dataset (http://www.esrl.noaa.gov/psd/) used in this paper covers the period from January 1948 to December 2013. The dataset gives both zonal and meridional components of

Table 1. Geographical location, recording period and summary of statistical characteristics of the ground stations.

Station	Lat. (N)	Long. (E)	Elevation (m a.s.l.)	Recording period	Years	Mean ($m\,s^{-1}$)	STD ($m\,s^{-1}$)
Abu Dhabi	24°26	54°39	27	1984–2013	30	3.67	1.06
Dubai	25°15	55°22	19	1984–2013	30	3.58	1.07
Al Ain	24°15	55°37	265	1995–2013	19	3.89	1.02
Fujairah	25°06	56°20	46	1996–2013	18	3.14	1.62
Ras Al Khaimah	25°37	55°56	31	1984–2013	30	2.33	0.91
Sharjah	25°20	55°31	34	1984–2013	30	3.00	0.95

surface wind speed at a height of 10 m and a spatial resolution of $2.5^\circ \times 2.5^\circ$ at three different temporal resolutions (4-times daily, daily and monthly). In accordance to the climate oscillation data, the monthly reanalysis data is used in the current work.

3.3. Climate oscillation data

Climate oscillations indicate the large scale, dynamic ocean and atmospheric circulations that result in climate patterns characterized by recurring cyclical fluctuations within global or regional climate at different time scales. Climate indices are the 'parameters' used to measure the values of such fluctuations. These parameters are mostly measured from anomalies in sea surface temperature, air pressure or solar radiation. The current work covers some of the major global climate oscillations in order to determine their influence on the wind speed in the UAE and ultimately to use them as possible predictors. These oscillations have different periodicity that enable both short-term and long-term interpretations of climate and wind speed variables in the region of interest. The data period and the links to the data source for each climate index are provided in Table 2.

4. Research methods

The methodology adopted in this work uses different statistical methods that include the following analyses.

4.1. Pearson's correlation coefficient

Correlation coefficient describes the linear dependence between two variables and helps understand how well the two variables are related by providing the magnitude (strength) and the sign (direction) of the relationship. Although there are a number of methods that study the correlation, Pearson's correlation coefficient (PCC), one of the most commonly used methods, is adopted here. PCC, denoted by r, between two variables x and y, is defined as the covariance of the two variables divided by the product of their standard deviations:

$$r = \frac{n\sum xy - \left(\sum x\right)\cdot\left(\sum y\right)}{\sqrt{n\sum x^2 - \left(\sum x\right)^2}\sqrt{n\sum y^2 - \left(\sum y\right)^2}} \quad (1)$$

where n is the total number of observations in each variable. r^2, also known as the coefficient of determination in the case of linear regression, describes how much of the variance in y is explained by x. For a more general case, the coefficient of determination is evaluated using a different expression. The statistical significance of r is determined by testing the null hypothesis H_0: $r = 0$ (there is no correlation), against the alternative hypothesis H_1: $r \neq 0$ (there is correlation). The test statistic t_r is computed from:

$$t_r = r\sqrt{\frac{n-2}{1-r^2}} \quad (2)$$

The value of t_r is compared to the t distribution table with $n-2$ degrees of freedom. H_0 is rejected at a significance level of α if the absolute value of t_r is greater than $t_{(1-\alpha/2)}$.

4.2. Change point detection

4.2.1. *Centred cumulative sum method*

Change point is an instance in time before and after which the statistical properties of a time series differ and indicates the non-stationarity of the time series. The Centred cumulative sum (Cusum) method is a simple non-parametric approach which helps identify the time (year) the change had occurred. Cusum (C_t), for a time series x_i of length n at time t is given by:

$$C_t = \sum_{i=1}^{t}\left(x_i - \overline{x}\right), \quad t = 1, 2, \ldots, n \quad (3)$$

where $\overline{x}$ is the mean of the time series. Cusum transforms a given time series to values of C_t that have negative (positive) slope if x_i lies below (above) the mean. Rapid changes in direction of the C_t values indicate change points.

The statistical significance of the change point is assessed by applying the Student's t-test for the equality of the means of the data before and after the change point. The test is computed from:

$$t = \frac{\overline{x}_1 - \overline{x}_2}{\sqrt{\frac{s_1^2}{n_1} + \frac{s_2^2}{n_2}}} \quad (4)$$

where $\overline{x}_1$ and $\overline{x}_2$ are the mean of the data before and after the change point respectively; s_1 and s_2 are the standard deviations whereas n_1 and n_2 are the sample sizes in each respective data.

4.2.2. *Bayesian change point procedure*

The Bayesian procedure outlined by Seidou and Ouarda (2007) is followed in this work to identify the number,

Table 2. Major global climate indices used in the current study and their source of data.

Climate oscillation	Short name	Period	Source of data
North Atlantic Oscillation	NAO	1950–2013	http://www.esrl.noaa.gov/psd/data/correlation/nao.data
El Niño Southern Oscillation Index	SOI	1951–2013	http://www.cpc.ncep.noaa.gov/data/indices/soi
	Nino 3.4	1854–2013	http://climexp.knmi.nl/data/iersst_nino3.4a.dat
Pacific Decadal Oscillation	PDO	1900–2013	http://www.esrl.noaa.gov/psd/data/correlation/pdo.data
North Pacific Oscillation	NP	1899–2013	https://climatedataguide.ucar.edu/climate-data/north-pacific-np-index-trenberth-and-hurrell-monthly-and-winter
Indian Ocean Dipole	IOD	1958–2013	http://www.jamstec.go.jp/frcgc/research/d1/iod/DATA/dmi.monthly.txt
Atlantic Multi-decadal Oscillation	AMO	1948–2013	http://www.esrl.noaa.gov/psd/data/correlation/amon.us.data
East Atlantic Oscillation	EAO	1950–2013	http://www.cpc.ncep.noaa.gov/data/teledoc/ea.shtml
Mediterranean Oscillation 1 & 2	MOI1 and MOI2	1958–2013	http://www.cru.uea.ac.uk/cru/data/moi/moi1.output.dat http://www.cru.uea.ac.uk/cru/data/moi/moi2.output.da
Arctic Oscillation	AO	1979–2013	http://www.ncdc.noaa.gov/teleconnections/ao/

magnitude and position of change points. The procedure detects change points in the relationship between independent variables and a dependent variable. In the absence of independent variables, it detects changes in the time series of the dependent variable. For n observations and d independent variables, the dependent variable is represented by y_j (j =1, …, n), whereas x_{ij} (i = 1, …, d and j = 1, …, n) indicates the jth value of the ith independent variable. The multiple linear regression can be expressed by:

$$y_j = \sum_{i=1}^{d} \theta_i x_{ij} + \varepsilon_j \tag{5}$$

A thorough description of the mathematical formulation of the procedure and how it detects the number and position of change points are presented in Seidou and Ouarda (2007).

4.3. Trend analysis

4.3.1. Modified Mann–Kendall test

When a clear non-stationarity or trend are observed in wind speed data, this information must be taken into account in the assessment of future wind characteristics and wind energy potential (see for instance Hundecha *et al.* (2008)). Long-term trend in wind speed can be investigated using the Mann–Kendall test. The test was developed to assess trends in time series and is the most widely used trend analysis method for hydro-climatologic time series (Mann, 1945). This test has two main advantages. One, it is non-parametric and hence does not require the data to follow any specific distribution. Second, it is less sensitive to sudden changes because of the non-homogeneity in the data. A modified Mann–Kendall test was proposed to account for autocorrelation in the time series (Hamed and Rao, 1998) and has gained wide acceptance in the hydro-climatological community (Khaliq *et al.*, 2009a, 2009b). The modified Mann–Kendall test is adopted in this work.

4.3.2. Linear regression method of trend analysis

The linear regression of a random variable Y (in this case wind speed) on time X can be written as:

$$Y = \beta_0 + \beta_1 X \tag{6}$$

The regression coefficient β_1 (the slope) indicates the mean temporal change of the variable Y. Positive value of β_1 shows increasing trend whereas negative value shows decreasing trend. The test statistic for β_1 is used by testing the null hypothesis H_0: $\beta_1 = 0$ (absence of trend) against the alternative hypothesis H_1: $\beta_1 \neq 0$ (presence of trend) at a significance level of α. H_0 is rejected when the absolute value of the test statistic exceeds the critical value $t_{1-\alpha/2}$. The total change during the period of observation is obtained by multiplying the slope with the time duration.

4.4. Continuous wavelet transform

The CWT has been developed to address the shortcomings of Fourier transform which decomposes the signal (time series data) into a series of sinusoidal functions with varying frequencies giving the localization in frequency only. CWT, however, decomposes the signal into a number of wavelets enabling localization in both time and frequency (scale) by shifting and stretching the wavelet, respectively. The Fourier transformation $X(f)$ of a time series $x(t)$ revealing the information regarding the frequency content f is given by:

$$X(f) = \int_{-\infty}^{\infty} x(t)\, e^{-2\pi i f t} dt \tag{7}$$

The CWT of a given continuous signal $x(t)$ is defined as the convolution of x_n with the local basis function $\psi_{n,s}(\eta)$, which is the scaled, translated and normalized form of the mother wavelet $\psi_0(\eta)$, and is given by Torrence and Compo (1998):

$$W_n^x(s) = \int_{-\infty}^{\infty} x(t)\, \psi_{n,s}^{*} \mathrm{d}t \quad \text{and} \quad \psi_{n,s} = \frac{1}{\sqrt{s}} \psi_0 \left(\frac{t-n}{s} \right) \tag{8}$$

where s is the scale parameter, n is the translation (time localization) parameter, ψ_0 is the mother wavelet and the asterisk (*) denotes the complex conjugate of the wavelet. The mother wavelet used in this study is the Morlet function. The Morlet is often considered for most natural phenomena as it provides optimum balance between time and frequency localization and adequately describes the shape of non-stationary signals such as hydro-climatology (Jevrejeva *et al.*, 2003). Being a complex function consisting of a number of oscillation waves, the Morelet provides phase angle relationship and captures the oscillatory nature of a signal.

A discretized form of CWT for a discrete observations (x_n, $n = 1, \ldots, N$) with uniform time steps δt at finite number of locations is given by:

$$W_n^x(s) = \left(\frac{\delta t}{s}\right)^{\frac{1}{2}} \sum_{n'=1}^{N} x_{n'} \psi_o^* \left[\frac{\left(n'-n\right)\delta t}{s}\right] \tag{9}$$

where N is the time series length. The wavelet coefficient, ${W_n}^x(s)$ indicates the degree of similarity between the wavelet and the time series. In the transformation, lower values of s compress the wavelet to analyze high-frequency components whereas higher values dilate the wavelet to describe low-frequency components.

In CWT, there is a wraparound effect near the beginning and end of the time series during the convolution process as the wavelet runs off the edge. Hence, the time series is padded with zeros which reduce the variance of the time series near the edge resulting in the cone of influence (COI). The COI is taken as the area influenced by the padding (edge effects). Due to the COI, only periods smaller than $N/\left(2\sqrt{2}\right)$ are considered significant (Torrence and Compo, 1998; Grinsted *et al.*, 2004).

Wavelet power spectrum (WPS) gives a measure of the time series variance (power) at each time n and scale (period) s with times of large variance showing high power. WPS, which contains no phase information from the original function, is evaluated from:

$$\left|W_n^X(s)\right|^2 = W_n^X(s)\, W_n^{X*}(s) \tag{10}$$

Other quantities such as the global wavelet spectrum (GWS) have been derived from the wavelet transform to condense the large amount of information contained in the wavelet spectrum. GWS, which is calculated by averaging the power spectrum over all times (temporal averaging), determines the characteristic scales and is given by:

$$\overline{W}_n^2(s) = \sum_{n=1}^{N} \left|W_n(s)\right|^2 \tag{11}$$

4.5. Cross wavelet transform

The cross wavelet transform (XWT) shows regions in time-frequency space where the two time series show high common power. Given two time series X and Y with CWTs ${W_n}^X(s)$ and ${W_n}^X(s)$, respectively, their XWT ${W_n}^{XY}(s)$ is the product of the complex wavelet transform of the first time series and the complex conjugate of the second time series (Torrence and Compo, 1998):

$$W_n^{XY}(s) = W_n^X(s)\, W_n^{Y*}(s) \tag{12}$$

Two time series with a significant XWT signal can suggest causation and thus potential teleconnection. Confidence levels of the XWT are derived from the square root of the product of two chi-squared distributions. A thorough description of cross wavelet analysis can be found in Torrence and Compo (1998).

Although XWT is an important tool to investigate relationships between two time series, a cautious interpretation needs to be made in light of the original time series. As XWT is not a normalized measure, significant powers will be detected not only in the case of co-varying power but also in the case of an extreme high power in one of the time series. In contrast, even if the two time series co-vary, XWT may fail to indicate this relationship if the individual CWT of the time series shows low power. Thus, for significance testing of the inter-relation between two time series, it is recommended to apply wavelet coherence which addresses the drawbacks of XWT (Maraun and Kurths, 2004).

4.6. Wavelet coherence analysis

The wavelet transform coherence (WTC) detects regions where two time series co-vary in the time-frequency space, but they do not essentially have high common power. Unlike XWT, which measures the common power, WTC measures the intensity of the covariance of the two series in the time-frequency space (Jevrejeva *et al.*, 2003). As described by Torrence and Webster (1999), the WTC of two time series is given by:

$$R_n^2(s) = \frac{\left|S\left(s^{-1} W_n^{XY}(s)\right)\right|^2}{S\left(s^{-1}\left|W_n^X(s)\right|^2\right) \cdot S\left(s^{-1}\left|W_n^Y(s)\right|^2\right)} \tag{13}$$

where S is a smoothing operator. Wavelet coherence, whose value ranges between 0 and 1 inclusive, is similar to the traditional correlation coefficient, and can be conceptualized as a localized correlation coefficient in the time-frequency space.

The phase relationship in the time-frequency space is measured by the phase angle $\phi_n^{XY}(s)$ which gives the delay between two time series at time n and scale s (Torrence and Webster, 1999):

$$\phi_n^{XY}(s) = \tan^{-1}\left(\frac{\mathfrak{I}\left\{S\left(s^{-1} W_n^{XY}(s)\right)\right\}}{\mathfrak{R}\left\{S\left(s^{-1} W_n^{XY}(s)\right)\right\}}\right) \tag{14}$$

where $\mathfrak{I}$ is the imaginary component and $\mathfrak{R}$ is the real component.

XWT and WTC of two data series give complementary information. Wavelet coherence is particularly useful in cases where the two time series have low-wavelet power but still with high coherence. The statistical tests developed by Torrence and Compo (1998) are followed in this paper. In addition, the Monte–Carlo method described by

Grinsted *et al.* (2004) is employed to estimate the statistical significance at the 5% level. The degree of coherence is indicated by some patterns in different regions of the WTC plots showing that the two signals are correlated.

4.7. Model performance evaluation

The performance of a model shows how well the model represents a set of observations. It quantifies the difference between the observed values and the modelled values. In this study, the root-mean-square error (RMSE), relative RMSE (rRMSE), mean bias error (MBE), relative MBE (rMBE) and the adjusted coefficient of determination ($\overline{R}^2$) metrics have been used to assess the performance of the model (multiple linear regression) used. The relative values, rRMSE and rMBE, are used to account for the magnitude of the variable by standardizing the RMSE and MBE values with respect to the actual value of the variable. The mathematical expressions used to evaluate the model performance are:

$$\mathrm{RMSE} = \sqrt{\frac{1}{n}\sum\left(\hat{y}-y\right)^2} \tag{15}$$

$$\mathrm{rRMSE} = 100\times\sqrt{\frac{1}{n}\sum\left(\frac{\hat{y}-y}{y}\right)^2} \tag{16}$$

$$\mathrm{MBE} = \frac{1}{n}\sum\left(\hat{y}-y\right) \tag{17}$$

$$\mathrm{rMBE} = \frac{100}{n}\sum\left(\frac{\hat{y}-y}{y}\right) \tag{18}$$

$$\overline{R}^2 = 1-\frac{\sum\left(y-\hat{y}\right)^2}{\sum\left(y-\overline{y}\right)^2}\frac{n-1}{n-(k+1)} \tag{19}$$

where n is the sample size, y are the actual values, $\hat{y}$ are the estimated values, $\overline{y}$ is the mean of the actual values, n is the number of observations and k is the number of variables. The performance of the model is evaluated as satisfactory based on the proximity of the value of $\overline{R}^2$ to one and the proximity of the values of RMSE, rRMSE, MBE and rMBE to zero.

5. Results and discussion

5.1. Wind speed characteristics of the region

5.1.1. Spatial distribution of wind speed and wind vector

To examine the circulation of wind in the UAE and surrounding regions, the spatial distribution of the wind speed and direction obtained from the gridded reanalysis data are presented in Figure 2. As indicated by the vectors, the UAE has northerly and northwesterly wind blowing from the sea throughout the year. This is due to the fact that Shamal ('north' in Arabic) wind, which blows from north to south, is dominant in the Arabian Gulf. This wind has two distinct regimes: winter Shamal and summer Shamal. Winter Shamal is characterized by strong northwesterly winds and is a rare event punctuated by irregular gale winds. Summer Shamal, in contrast, is generally more stable but less significant in terms of its strength (Perrone, 1979).

Over the Arabian Peninsula, wind is mostly westerly. It originates from the Mediterranean Sea sweeping east across the northern part of the peninsula and flows down the Arabian Gulf before it turns west forming a clockwise circulation. In the southern part of the peninsula, the circulation is, however, reversed in the course of some months. In winter, the wind comes from the Gulf of Oman but in summer this pattern is reversed as the wind originates from the western part of the Indian Ocean resulting in a counterclockwise pattern. This observation was also reported in Nasrallah *et al.* (2001). In the northern part of the peninsula, nevertheless, the westerly wind originating from the Mediterranean persists throughout of the year.

5.1.2. Inter-annual variability and monthly climatology of wind speed

The annual wind speed intensity in each station and average wind speed intensity of all stations are presented in Figure 3. In contrast to the highest wind speed in Al Ain, Ras Al Khaimah experiences the lowest wind speed. Dubai and Abu Dhabi exhibit high and similar wind speed patterns till 2008. Although wind speed in Sharjah is low, it is stronger than in Ras Al Khaimah. The lowest wind speed in Ras Al Khaimah could be attributed to the proximity of the station to the Hajar Mountains. Wind speed in Fujairah shows peculiar behaviour with a clearly increasing trend and hence the highest variance of all the stations (see Table 1).

The seasonality shown in Figure 4, depicts the intra-annual variations of the wind speed in the stations in terms of the maximum, median and minimum wind speed. Higher wind speed is observed from the end of winter to the beginning of summer while in the remaining months, especially during autumn, it is lower with the exception of Fujairah which shows a different pattern with higher and lower wind speeds observed in summer and winter, respectively. In Abu Dhabi, Dubai and Al Ain, the monthly climatology reveals a slightly bimodal distribution of the wind speed with humps occurring in early spring and late summer. This seems to indicate the close association of the wind speed in these stations. Sharjah and Ras Al Khaimah, on the other hand, show a unimodal distribution with the highest wind speed prevailing in early summer in Sharjah and late summer in Ras Al Khaimah. The months show also different wind speed variations. Seasons of high-wind speed generally experience high variation while low variation is recorded in seasons of low-wind speed. The highest and lowest variations are observed in March and September, respectively.

5.2. Correlation results

With the exception of NP and MOI, which exhibit high correlation with wind speed in Abu Dhabi, all other indices

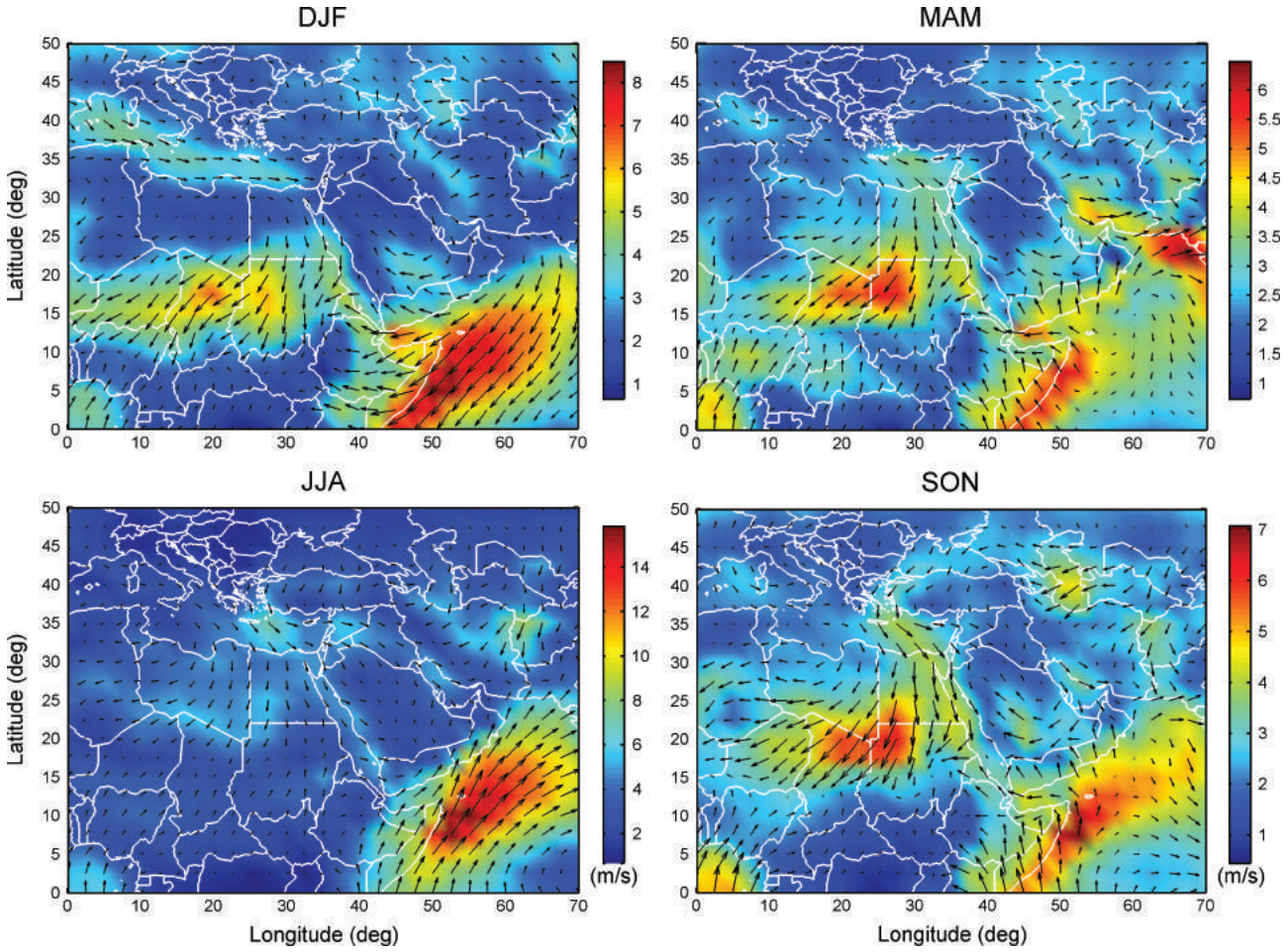

Figure 2. Spatial distribution of wind speed and wind direction during different seasons.

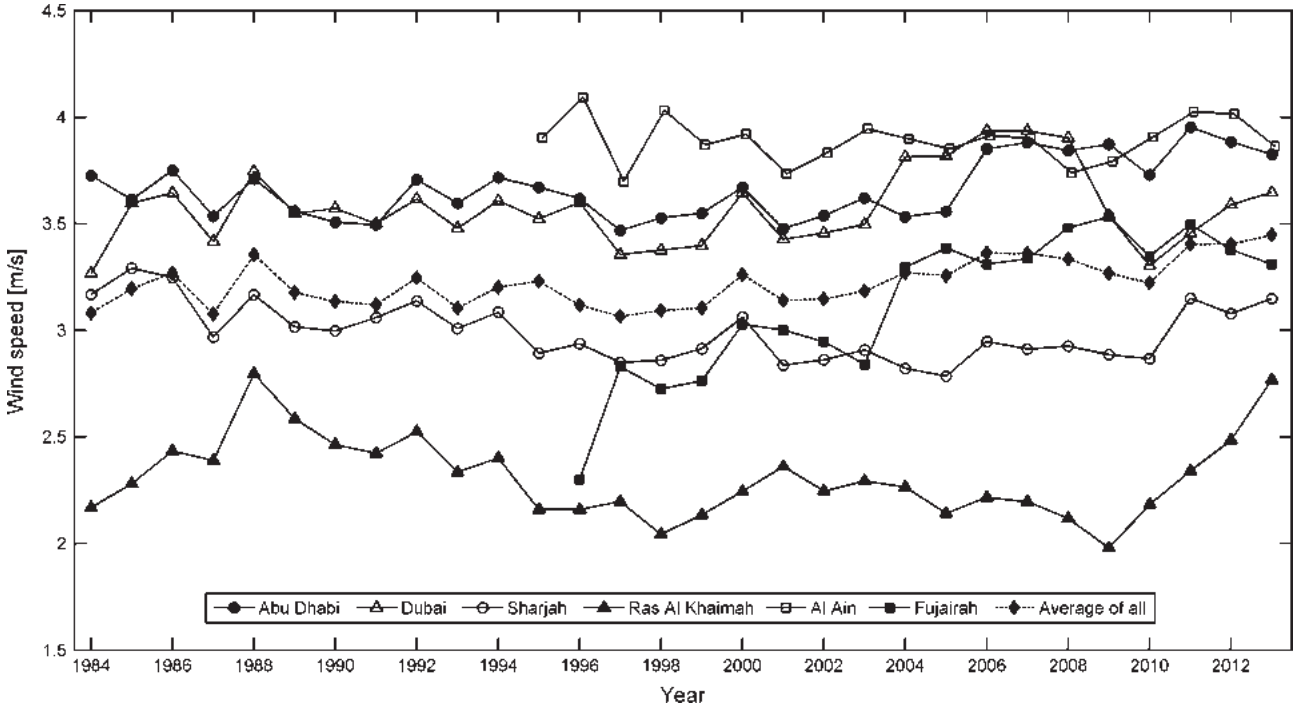

Figure 3. Annual wind speed in each ground station and average wind speed of all stations.

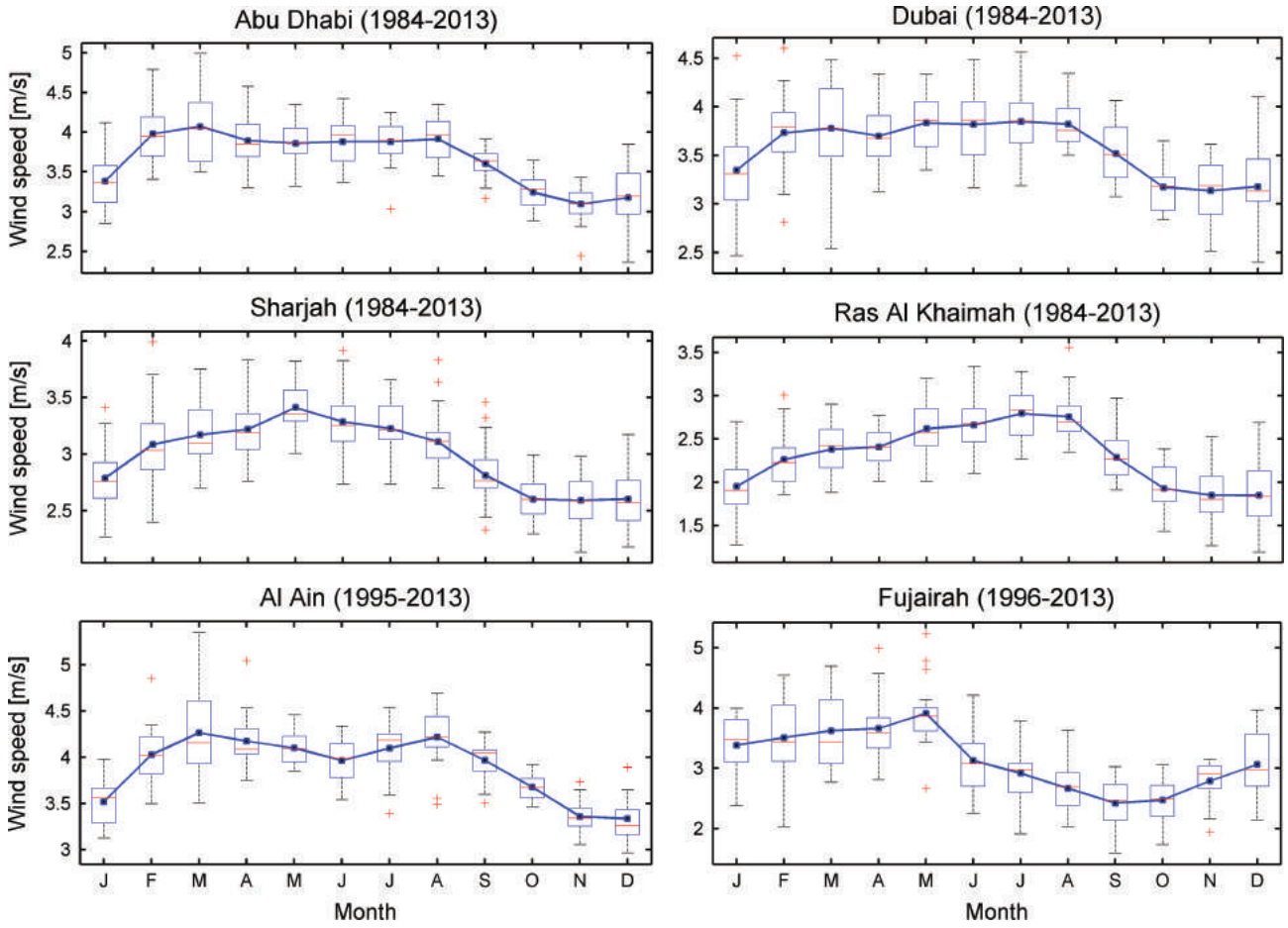

Figure 4. Seasonality of the wind speed in each ground station.

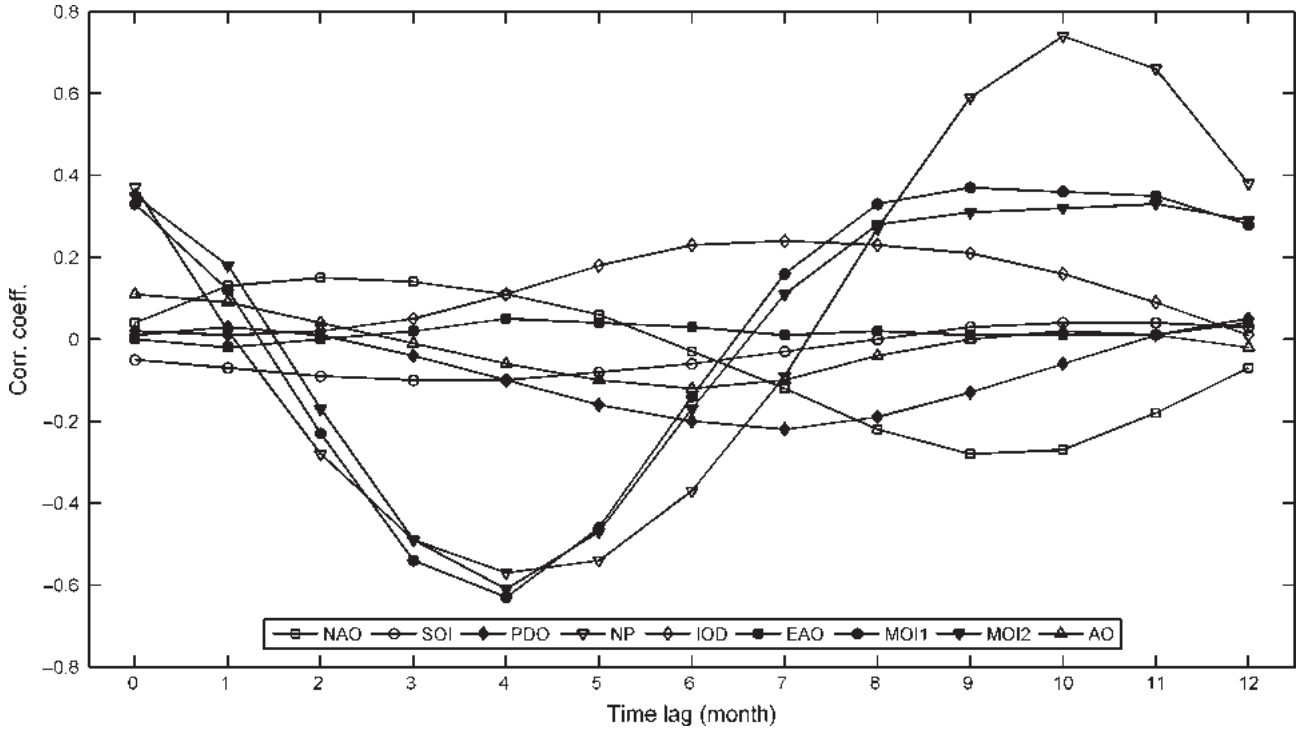

Figure 5. Correlation values between the 3-month wind speed in Abu Dhabi and the corresponding climate indices at different time lags.

show low correlation. Correlation coefficients observed at a significance level of 95% range from 0.12 to 0.74 explaining as high as 55% of the wind speed variation. Although other indices also show statistically significant correlation coefficients, the values are too low to give meaningful explanation for the wind speed variations. The high correlation values exhibited by the NP and MOI indices are basically capturing the seasonality as opposed to the actual wind speed pattern. This is the reason why the correlation values are swinging from negative to positive (Figure 5) as the size of the lags between the indices and the wind increases, indicating in-phase and anti-phase relationship expressed by the negative and positive correlation values, respectively.

5.3. Change point detection results

5.3.1. Cusum method

From the Cusum result of each station, the change points are visually identified and their statistical significance is evaluated by conducting the Student's *t*-test for change in the mean wind speed before and after the change point. All stations, with the exception of Al Ain, reveal at least one change point. The statistical significance of the identified change points is estimated at the significance levels of 1 and 5%. By comparing these results to the results of change point analysis for the various climate indices, associations were made between wind speed and climate indices based on the year of occurrence of the change points. The year of occurrence of the change points, the statistical significance level and the indices likely associated with the change points are summarized in Table 3.

Table 3. Summary of change point analysis.

Stations	Change point at (year)	Significance level (%)	Indices possibly associated with the change point
Abu Dhabi	2006	1	NP and IOD
Dubai	2004	5	SOI, EAO and PDO
Sharjah	1995	1	NAO, SOI, AMO, MOI1 & 2 and AO
Ras Al Khaimah	1995	5	NAO, SOI, AMO, MOI1 & 2 and AO
Fujairah	2004	1	SOI, EAO and PDO

5.3.2. Bayesian procedure

The Bayesian approach was employed to detect the change points and compare them with those of the Cusum method. Results of this approach presented in Figure 6 also coincide with the results of the Cusum method. With

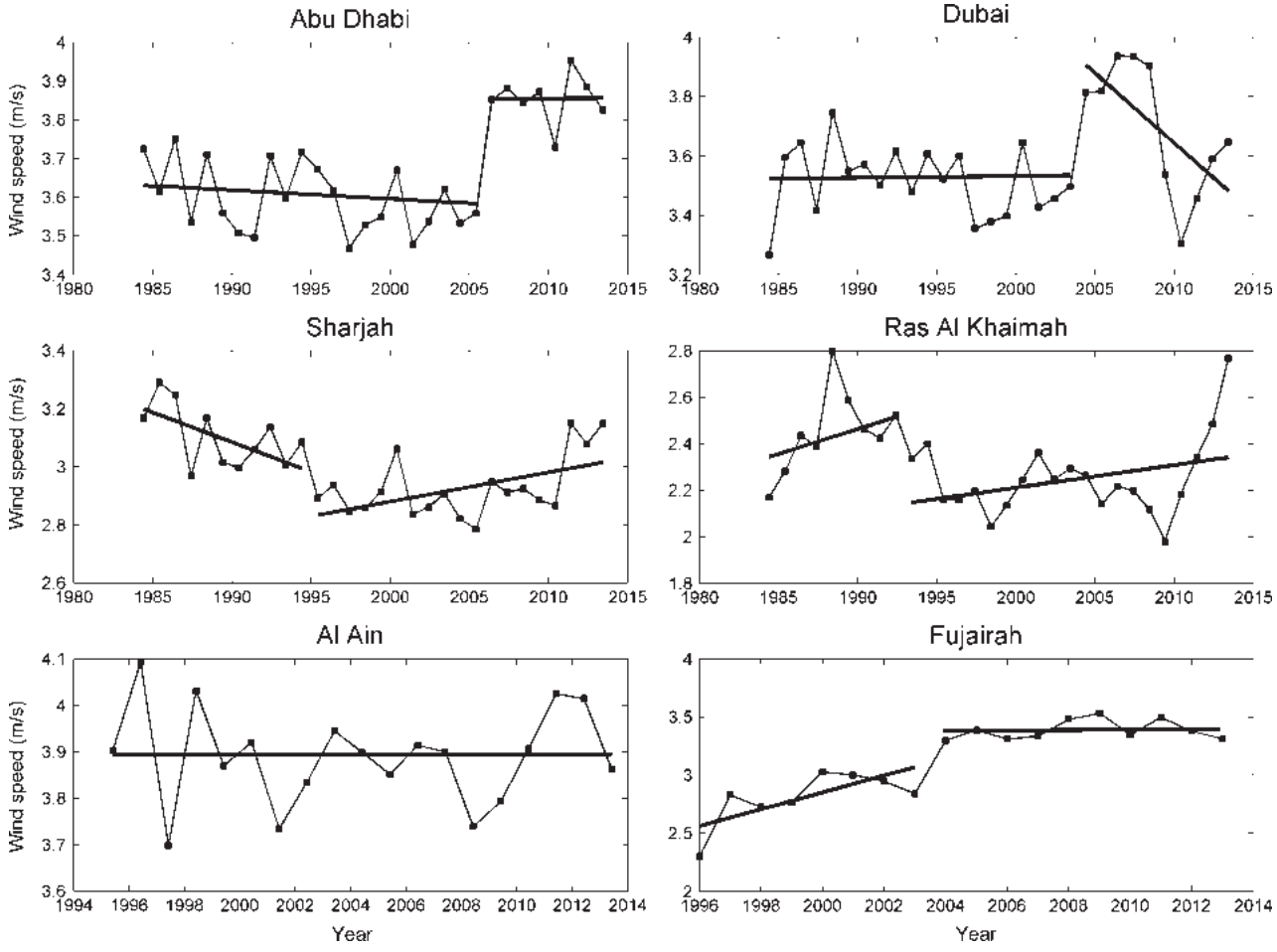

Figure 6. Results of the Bayesian change point detection procedure.

Table 4. Mann–Kendall test result for the presence of trend in wind speed in each month.

Station	January	February	March	April	May	June	July	August	September	October	November	December
Abu Dhabi	Yes	No	No	Yes	No	Yes	No	Yes	No	Yes	Yes	Yes
Dubai	No	No	No	No	No	No	No	No	No	Yes	Yes	No
Sharjah	No	No	No	No	Yes	Yes	No	Yes	No	Yes	Yes	No
Ras Al Khaimah	Yes	No	No	No	No	No	No	No	No	No	No	No
Al Ain	No	No	No	No	No	No	No	No	No	No	No	No
Fujairah	Yes	Yes	Yes	Yes	Yes	Yes	Yes	Yes	Yes	Yes	Yes	Yes

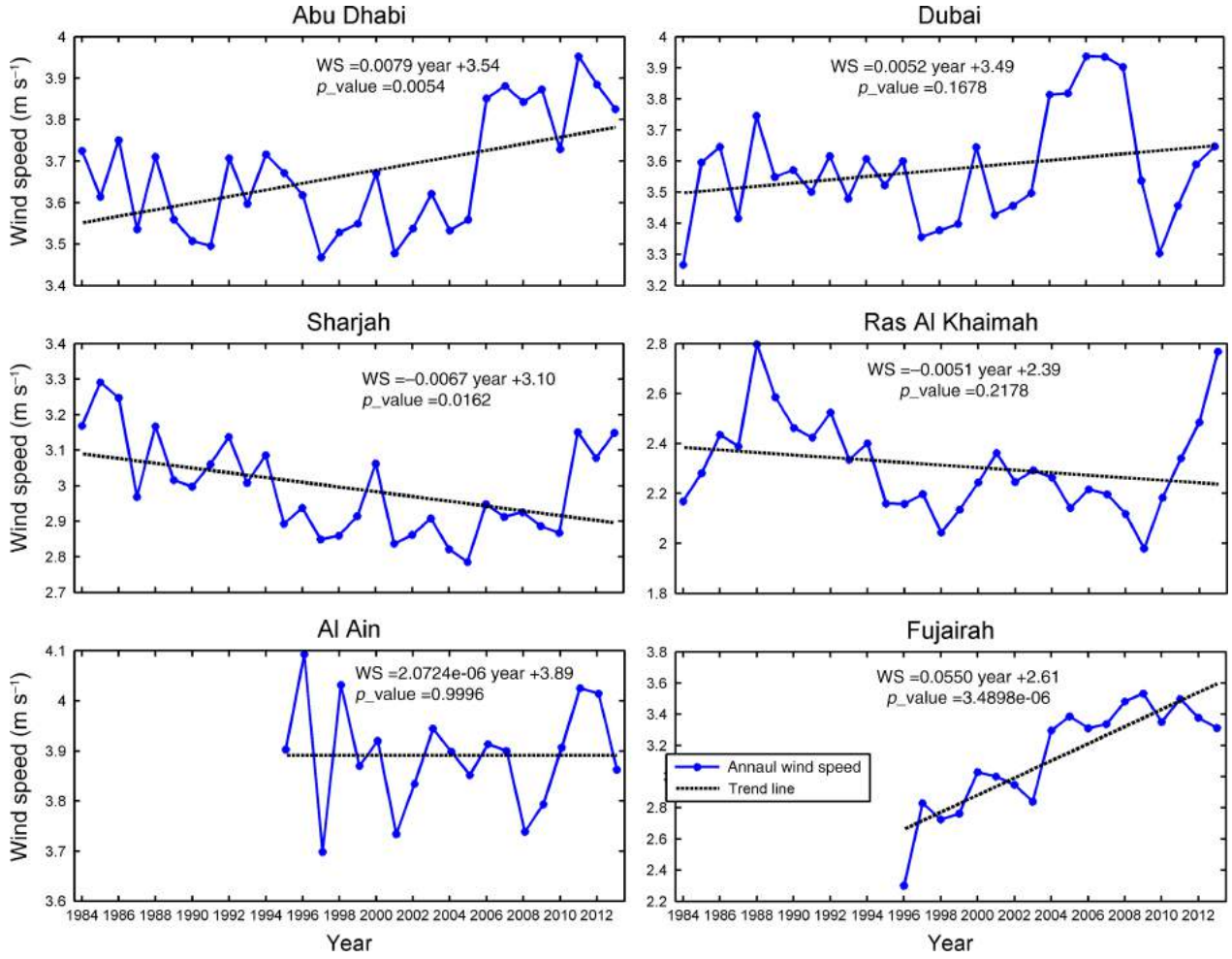

Figure 7. Trend analysis using linear regression method.

the exception of the Ras Al Khaimah station which shows a change point in 1993 instead of 1995, all other stations indicate the same instance of change point as presented in Table 3. Most of the stations show change point in 1995 or 2004.

5.4. Trend analysis results

5.4.1. Modified Mann–Kendall test

Using the modified Mann–Kendall test (with $\alpha = 0.05$), monthly (wind speed of a particular month taken from each year of the record period) and annual wind speed time series at all stations are assessed for the presence of trend. As shown in Table 4, a significant positive trend is observed in Fujairah for all months as opposed to Al Ain, which does not show trend in any of the months. Ras Al Khaimah shows trend in 1 month only (January) whereas Dubai shows trend in 2 months. Abu Dhabi and Sharjah, however, show trends in few months.

The same test is also carried out on annual wind speed data. Annual wind speed in Abu Dhabi, Sharjah and Fujairah show significant trends at the 5% level. It is observed that wind speed in Abu Dhabi and Fujairah is increasing in contrast to wind speed in Sharjah which is showing a decreasing trend. Wind speed in Dubai, Ras Al Khaimah and Al Ain do not show statistically significant trends. Stations that show significant trends in several months (Table 4) are found to exhibit significant trend in the annual wind speed as well.

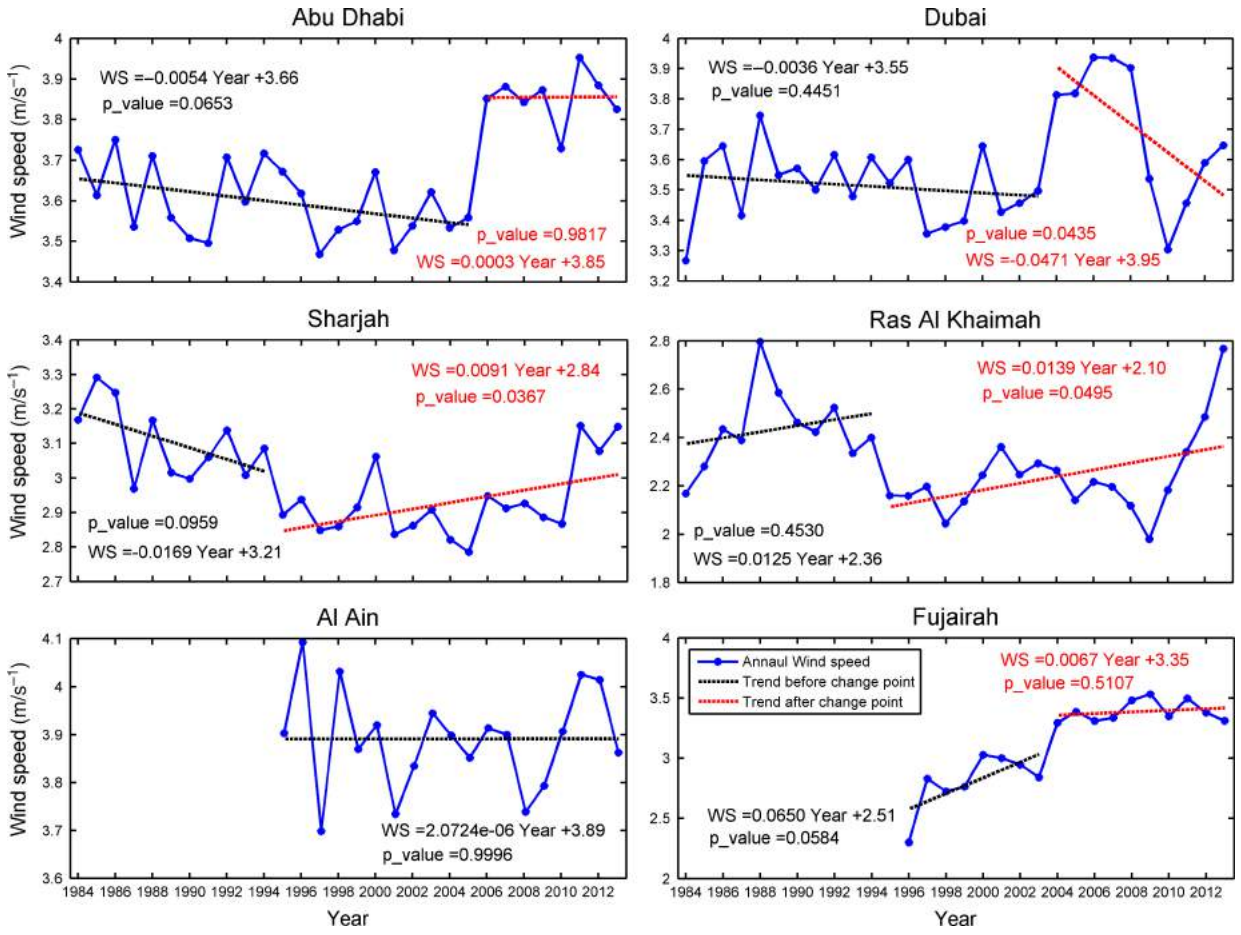

Figure 8. Trend analysis before (in black) and after (in red) the change point.

5.4.2. *Linear regression method*

Linear regression was also used separately to perform trend analysis on the annual wind speed data and the result is shown in Figure 7. Although the regression lines for all stations, except Al Ain, seem to show either a decreasing or increasing trend, their statistical significance is checked by calculating the p value of the slopes. Trends in Dubai, Ras Al Khaimah and Al Ain are insignificant at the 5% level as the p-values for these stations are greater than 0.05. The remaining stations, however, show statistically significant trends. Sharjah exhibits a decreasing trend at the 5% significance level whereas Abu Dhabi and Fujairah show an increasing trend at the 1% level. The results of this method confirm what has been observed with the modified Mann–Kendall test.

For stations that show distinct change points, further trend analysis is done by considering the data before and after the change point separately. The outcome of this analysis is presented in Figure 8 and a different scenario from the case which did not consider the change points emerged. Stations, which have shown a monotonic statistically significant (at the 5% or less) increase or decrease of wind speed when the whole data was considered, such as Abu Dhabi and sharjah, now show two different trends although all the trends are not significant at the 5% level. At a significance level of 5%, wind speed in Dubai shows a decreasing trend after the change point while in Sharjah and Ras Al Khaimah, it shows an increasing trend. Interestingly, no station shows a statistically significant trend at the 5% level before the change point.

5.5. Wind speed periodicity

To determine the dominant frequency of wind speed, both wavelet and Fourier transform were performed. The CWT power spectrum and the GWS of the monthly wind speed time series are shown in Figure 9. The 95% confidence interval enclosing the high variance in the CWT and the corresponding peak in the GWS shows that the significant and dominant period in all stations is 1 year (annual). In addition to the annual periodicity, wind speed in Abu Dhabi, Al Ain and to some extent in Dubai shows half-yearly (biannual) periodicity. The biannual periodicity observed here corresponds to the slight bimodal pattern observed in Figure 4. No significant higher periods are identified in any of the stations though.

Similar analyses were carried out using the Fourier transform for comparison, as depicted in Figure 10. The horizontal axis represents the frequency (f) and the vertical axis shows energy or variance at the corresponding frequency. High energy is recorded in all stations at a frequency $f \approx 0.002747\ \text{day}^{-1}$. This frequency corresponds

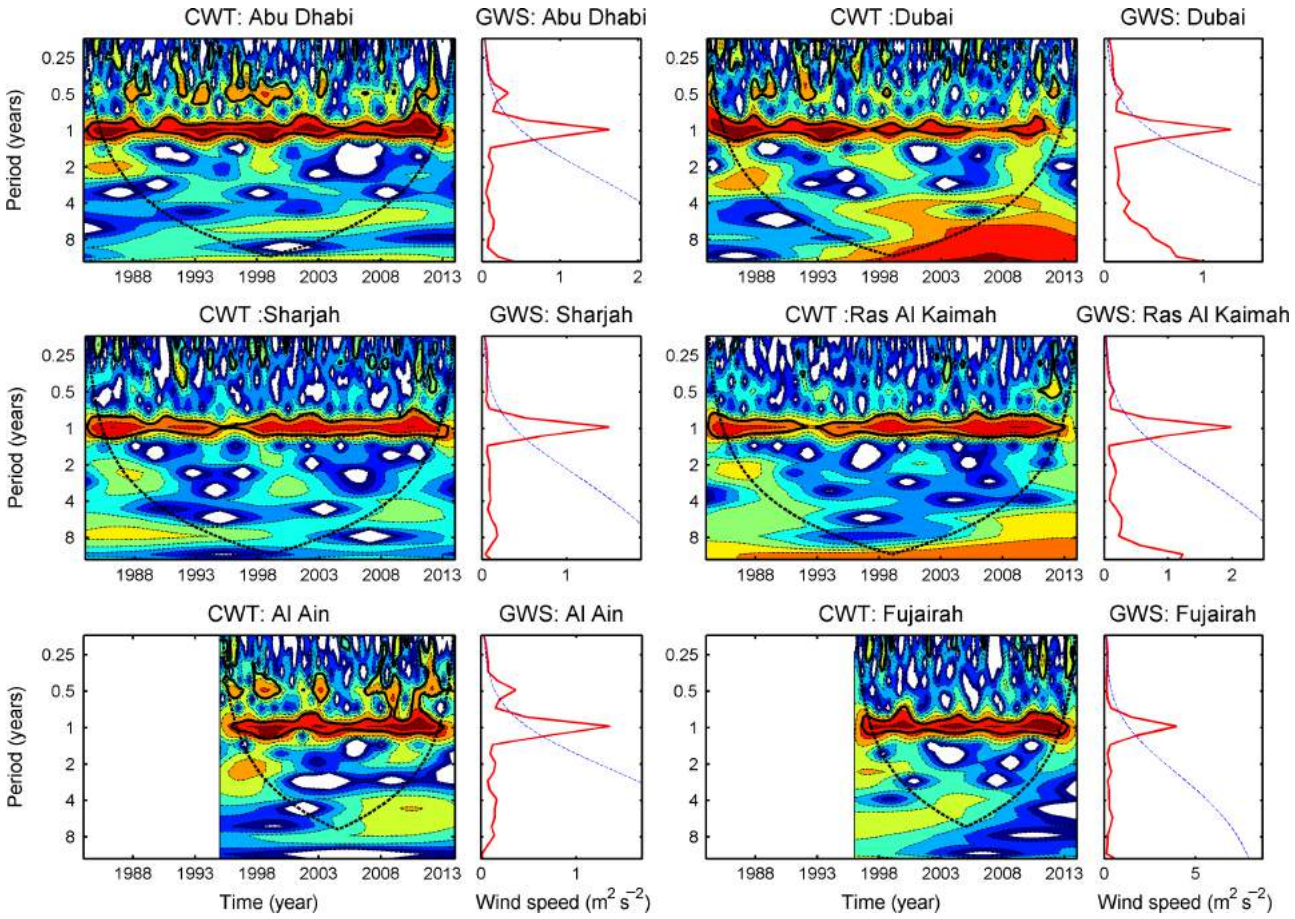

Figure 9. Continuous wavelet transform (CWT) power spectrum and corresponding global wavelet spectrum (GWS) of monthly wind speed. Black solid contour lines in the CWT enclose peaks of greater than 95% confidence for a red noise process. The curve (broken black line) depicts the COI where the edge effects become important. The dashed blue line in the GWS shows the 95% confidence level.

to a period of 364 days, which is roughly equivalent to 1 year, consistent with the results of the CWT. Another peak is also noted around $f \approx 0.00554\,\text{day}^{-1}$ which represents biannual periodicity. This peak is clearly distinct in Abu Dhabi, Al Ain and Dubai reflecting the findings of the continuous wavelet analysis. No other significant lower frequencies corresponding to higher periods are detected in this transform. This confirms also the fact that wind speed does not show longer periodicities other than the yearly and half-yearly.

5.6. Wavelet coherence analysis results

5.6.1. Ground station wind speed data

*WTC was performed for annual 3-month data (3 month average data from each recording year) to examine the time of coherence as well as the phase relationship between climate indices and wind speeds. As shown in Figure 11(a), the NAO index shows strong coherence with the wind speed in Abu Dhabi during the months of May–June–July in the time period of 6–7 years from 1991 till 2003. Both signals are in-phase indicating positive correlation. The in-phase relationship implies that a positive phase of the index results in higher wind speed. Swings in the phase of NAO and their effect on wind speed in the northern hemisphere have already been reported by Hurrell and Deser (2010). The NAO WTC analysis result is consistent with the findings of Hurrell (1995) which indicated a relationship between the positive phase of NAO and stronger than average westerly winds across the middle latitudes swiping in the west–east direction. The influence of the NAO on the Middle East climate was also documented by Cullen *et al.* (2002).

Wind speed in Abu Dhabi exhibits significant coherence with SOI during September–October–November with a 5–6 years period in the years 1992 to 2004 with in-phase relationship (Figure 11(b)). Similar results, in terms of periodicity, but with opposite phase relationship are observed for the Nino 3.4 index (Figure 11(c)). This is because SOI and Nino 3.4 have strong negative correlation. During the rest of the autumn months and winter, significant coherences are also observed between wind speed and both SOI and Nino 3.4 indicating the influence of ENSO during these seasons. The phase relationship confirms that when SOI is in positive phase (La Niña), wind speed in Abu Dhabi picks up and during the negative phase of SOI (El Niño) wind speed decreases as the pressure gradient weakens because of the warming of the Arabian Gulf as explained by Nazemosadat *et al.* (2006).

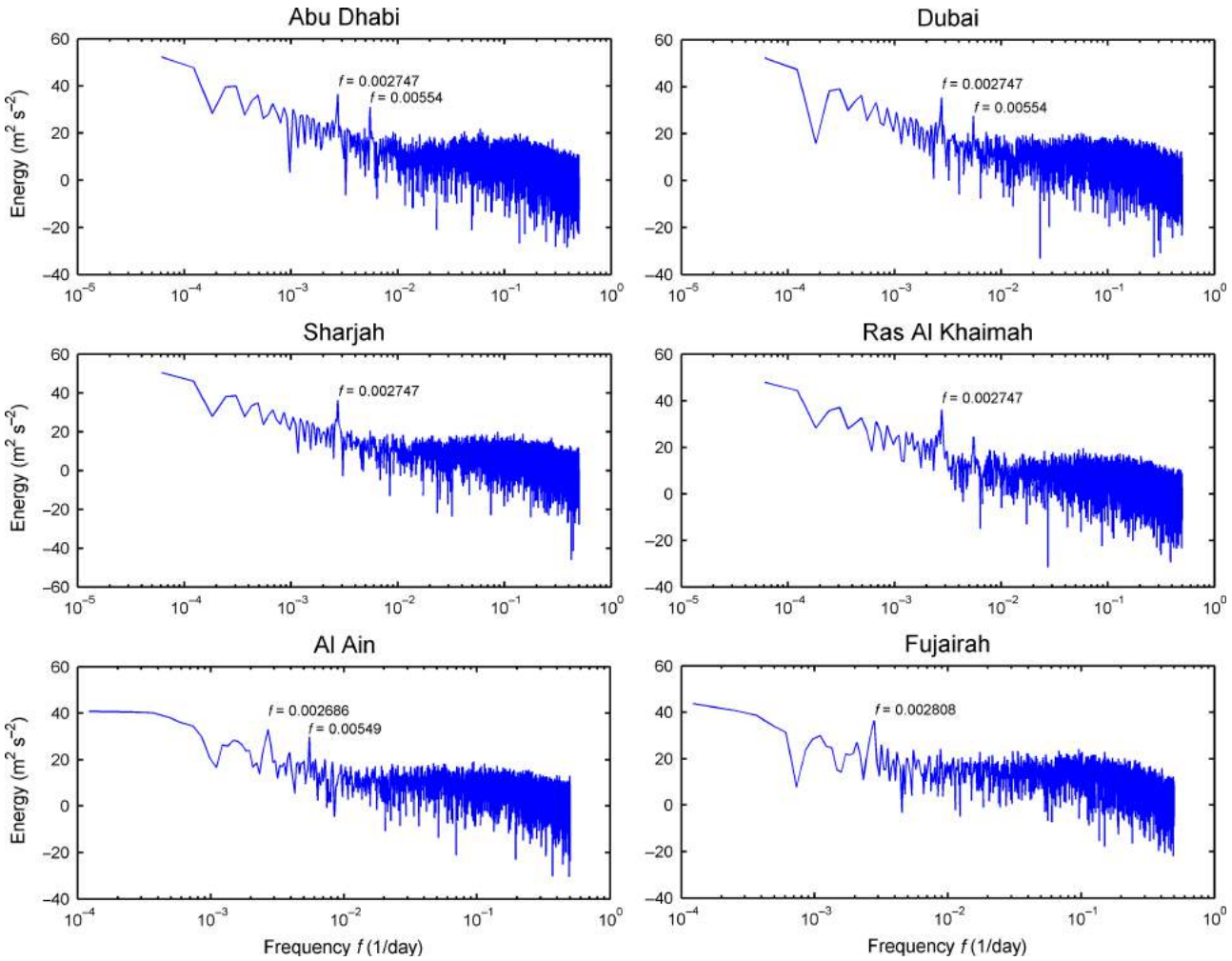

Figure 10. Fourier transform power spectrum of ground stations' wind speed.

Similarly, PDO exhibits negative coherence with periods of 5–7 years but during August–September–October from the year 1998 to 2005 (Figure 11(d)). The anti-phase relationship is clearly indicated by the arrows pointing to the left. The negative coherence indicates that the high (warm) phase of PDO results in low-wind speed which has also been observed during the El Niño period (low phase of SOI). A positive relationship between PDO and ENSO was already established (Zhang *et al.*, 1997; Oliver, 2012). Accordingly, the high phase of PDO occurs during El Niño periods during which the western Pacific becomes cooler than the eastern part and the event is reversed during La Niña (low phase of PDO). The result of WTC analysis obtained here replicates the positive relationship between the two indices.

As can be seen in Figure 12(a), IOD reveals strong coherence in the 2–3 years period during November–December–January in the late 1990s and early 2000s; both signals exhibiting an in-phase coherence. This coherence demonstrates the positive influence of IOD during the winter months. Similar to PDO, IOD is associated with ENSO and accordingly positive IOD events are connected to El Niño episodes (Saji and Yamagata, 2003). The result here, however, does not support this association as high wind speeds are related to the positive phase of IOD. In addition, Figure 12(b) indicates significant coherence between EAO and wind speed in Abu Dhabi at the 7 years period during August–September–October from 1992 to 2002. During this time both signals are in-phase with EAO slightly leading wind. The in-phase relation indicates that during positive (warm) phases of EAO, wind speed in Abu Dhabi increases. The result is similar to the correlation found between wind speed and the phases of NAO. EAO is structurally similar to the NAO (Barnston and Livezey, 1987) and the outcome of the WTC analysis is in line with this similarity.

Results of wavelet coherence analysis for MOI indicate also a stronger relationship with MOI1 than with MOI2. As shown in Figure 12(c), MOI1 demonstrates strong coherence during the months of July–August–September with 6–7 years period from 1992 to 2005 and 2 years period around 2000. An in-phase relationship is observed between the two signals. This positive association between MOI and wind speed may indicate the influence of NAO on MOI oscillation as reported by Criado-Aldeanueva and Soto-Navarro (2013). In addition, AO (Figure 12(d)) shows significant coherence during the months of

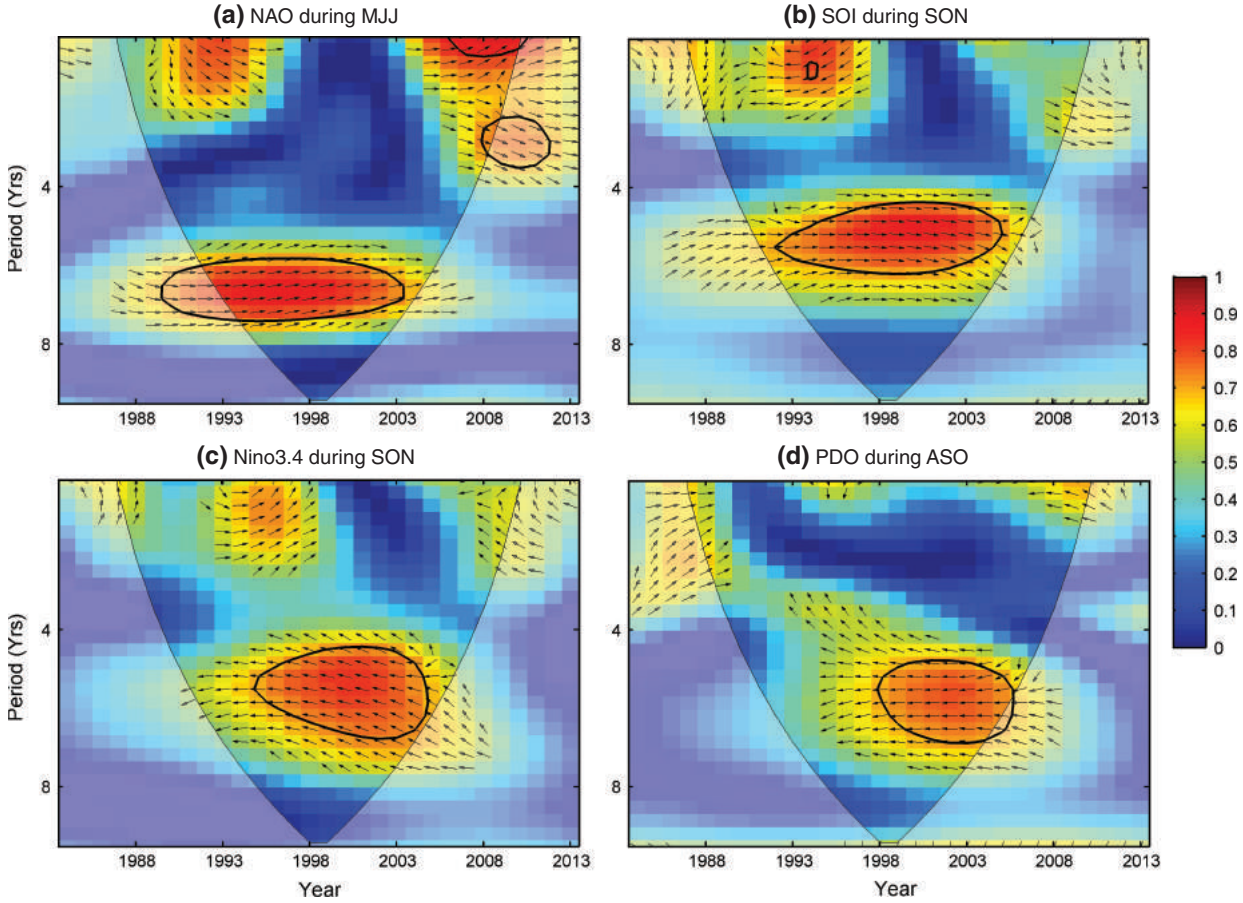

Figure 11. WTC analysis and phase difference of wind speed in Abu Dhabi with: (a) NAO index during the months MJJ, (b) SOI during SON, (c) Nino 3.4 during SON and (d) PDO during ASO. The thick black contour is the 5% significance level against red noise. The vectors indicate the phase difference between climate index and wind speed. Vectors pointing right (left) show in-phase (anti-phase) relationship. The thin black curve represents the COI. The strength of the coherence is indicated by the colour.

September–October–November at a period of 5–7 years for an extended length of time (1991 to 2006) with an in-phase relationship.

For wind speed in Dubai, NAO reveals (figure not shown) strong coherence during the months of August–September–October in the 3–4 years period starting from 1995 to 2007. SOI also indicates strong positive coherence with wind speed at a period of 4–6 years during the months of October–November–December from the year 1993 until 2006. In the same season and years, Nino 3.4 reveals significant coherence during the months of September–October–November. The periodicity of the association observed here is consistent with the cycle of ENSO, which generally ranges from 2 to 7 years (Torrence and Webster, 1999). Wind speed in Dubai also shows strong but short coherence with EAO during August–September–October. The results of the coherence analyses of wind speed in Dubai with the various climate indices are in agreement with those of Abu Dhabi.

Wind speed in Sharjah and Nino 3.4 display opposite phases in the 5–6 years period with significant coherence extending from 1992 to 2005. NAO displays high coherence with the wind in Sharjah in the 6–7-year period during May–June–July from 1993 to 2004. This period for NAO is consistent with the variability of the index which is centred on 6–10 years and 2–3 years as noted by Cullen *et al.* (2002). Furthermore, wind speed in Ras Al Khaimah reveals strong coherence in excess of 0.9 with EAO during the summer months. The same station also shows strong coherence with IOD during the autumn months. Although the recording length is short, wind speeds in Al Ain and Fujairah also display significant coherence with NAO and EAO.

From the wavelet coherence analyses between the wind speeds and the various climate indices, ENSO, IOD, PDO and AO influence the autumn and winter wind speed with varying periodicity but largely at a band ranging from 3 to 7 years. Summer wind speed is mainly affected by NAO, EAO and MOI with a periodicity of 5–7 years. These indices have been found to influence the hydro-climatological variables of this region as was established by a number of studies (Charabi and Abdul-Wahab, 2009; Bannayan *et al.*, 2010; Almazroui, 2012; Niranjan Kumar and Ouarda, 2014; Chandran *et al.*, 2015).

5.6.2. *NCEP/NCAR gridded reanalysis wind speed data*

Figure 13 shows the spatial variation of the wavelet coherence between the reanalysis wind data (1984–2013)

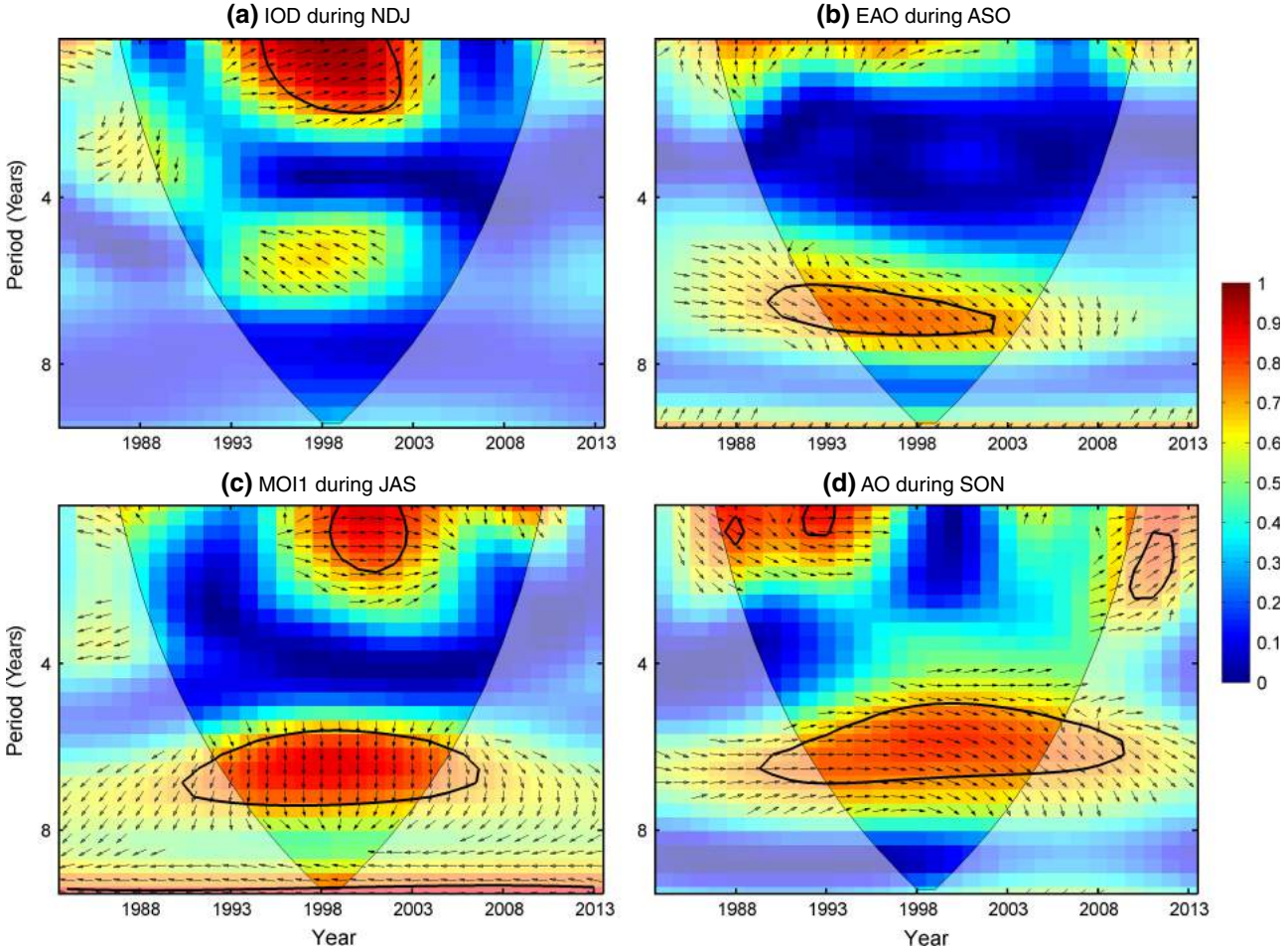

Figure 12. Same as Figure 11 but with (a) IOD during the months NDJ, (b) EAO during ASO, (c) MOI1 during the JAS and (d) AO during SON.

over the UAE and surrounding region and Nino 3.4 during October–November–December. Strong coherence is observed in two distinct periods. The first is in the 2–4 years period especially in the southern part of the region from the end of 1980s to the early 2000s in which both signals display in-phase relation indicating positive correlation. The second is in the 4–8 years period which is more prevalent in the northwestern part of the region and appears to occur during the entire recording time. Here the two signals are out of phase and hence negatively correlated. These two periods are consistent with the 2–7 years period of ENSO (Torrence and Webster, 1999). Significant coherence is observed over the entire Arabian Gulf because of the strong influence of ENSO on this region (Nazemosadat and Cordery, 2000; Marcella and Eltahir, 2008; Niranjan Kumar and Ouarda, 2014; Chandran *et al.*, 2015).

It is noteworthy to mention that, for a 30-year time series data due to the COI the longest periodicity that can be observed is 10 years [$\approx 30/(2*2^{0.5})$ (Torrence and Compo, 1998)]. Such short time series data, therefore, might not give the full extent of the coherence analysis. Hence a longer time series data, for both the index (Nino 3.4) and the reanalysis data during the same months (October–November–December), stretching from 1948 to 2013 are taken for comparison with that of 1984 to 2013. The resulting WTC displaying the spatial variation during these years is shown in Figure 14. In addition to the two periods of high coherence (2–4 years and 4–8 years) identified in Figure 13, another strong coherence with a longer period of 12–16 years having in-phase relationship is observed in the southern part of the region. Besides, the 4–8 years period that was observed to be occurring continuously in Figure 13 can now be seen to be confined from the early 1980s to 2013.

5.7. Partial correlation and step-wise regression

Partial correlation, which is the correlation between the predicted variable and one of the predictor variables after the effect (common variance) of all other predictor variables over that has been removed, has first been assessed to check multicolinearity and interdependence between the predictors at different lags. NP at lag-10 (wind speed lagging the index by 10 months) is, for instance, found to be highly correlated with NP at lag-4 and hence the influence of NP at lag-4 is effectively accounted for by NP at lag-10. Only those indices that show higher correlation values have been adopted. Following step-wise regression to select the best predictors for the wind speed, NP at lag-10, MOI1 at lag-4 and NAO at lag-9 are taken as predictor variables. The model performance is assessed

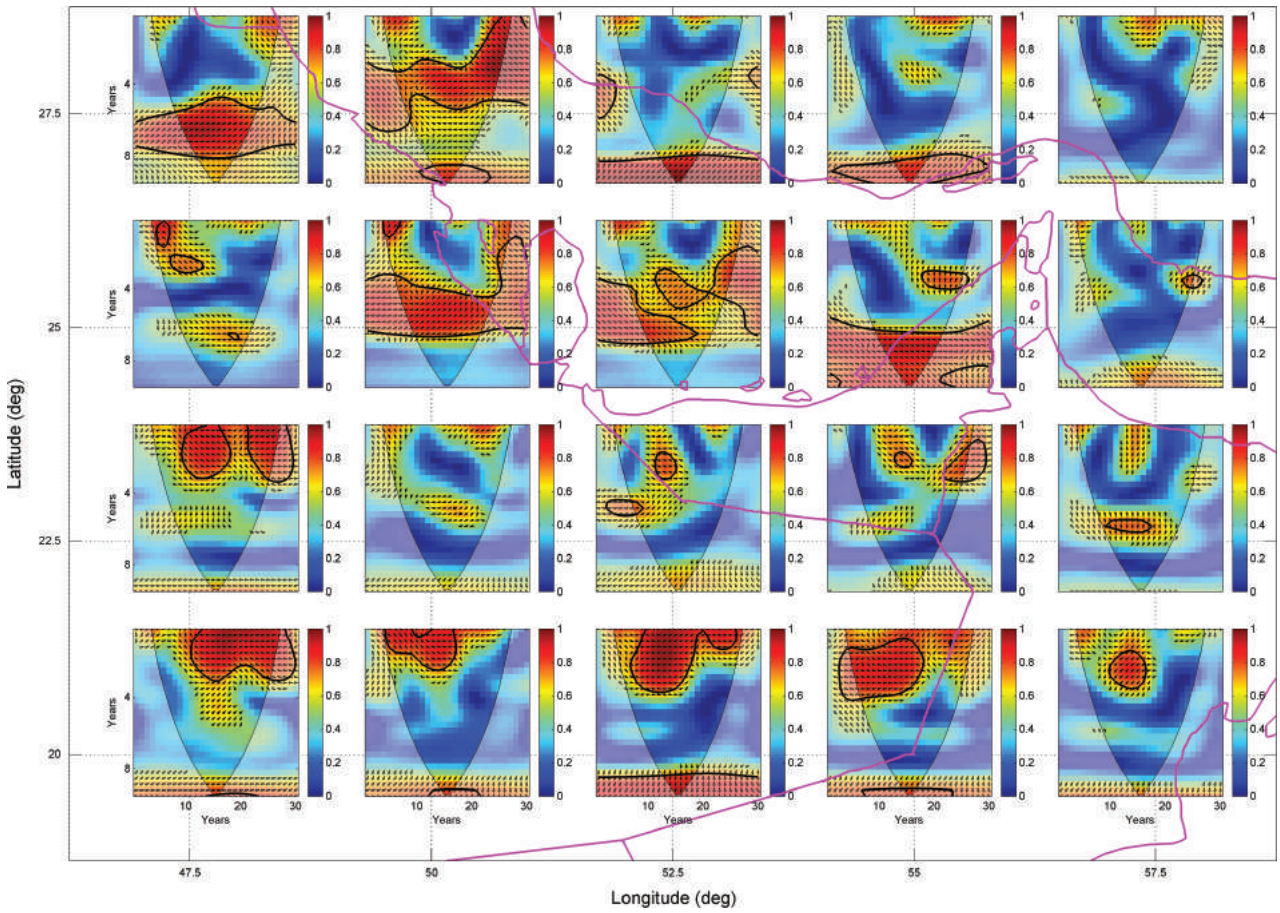

Figure 13. Spatial variation of WTC of the NCEP/NCAR reanalysis wind speed over the UAE and surrounding regions with Nino 3.4 during OND for the years 1984–2013. The thick black contour shows the level of significance at 5%. The thin black curve represents the COI. The magenta line indicates international borders and coastal lines.

using RMSE, rRMSE, MBE, rMBE and adjusted coefficient of determination which gave values of 0.21 m s^{-1}, 5.9%, 0.001 m s^{-1}, −0.35% and 0.63, respectively. The RMSE helps to combine the discrepancies between values estimated by a model and the actual observed value, i.e. the residuals, into a single estimate of predictive power and a value of 0.21 m s^{-1} is reasonably acceptable. The MBE is close to zero, which is equivalent to the required ideal value, indicating the overall lack of bias. A positive value of MBE gives the average amount of over-estimation in the modelled variable while a negative value indicates underestimation. The model has, however, sytematically underestimated higher wind speeds while overestimating lower wind speeds. Though the model is not able to capture the relative extremes of wind speed, it is able to explain over 63% of the wind speed variance.

6. Conclusions

Long-term variability of wind speed in the UAE was explored using wind speed data collected from six ground stations. Individual stations were investigated for inter-annual and intra-annual variation. With the exception of Fujairah all stations displayed similar intra-annual variation. Trend analysis was also performed to investigate the existence of trends and change points. Results indicated that half of the stations have a significant trend at the 5% significance level and with the exception of one station (Al Ain), all stations exhibited change points with statistical significance of at least 5%.

Wind speed revealed annual periodicity in all ground stations and biannual periodicity in three stations: Abu Dhabi, Al Ain and Ras Al Khaimah. Wavelet analysis (both WTC and XWT) using the Morlet function was carried out for annual 3-monthly moving average wind speed and the various climate indices. It was observed that the region's wind speed is mostly affected by four indices namely ENSO, NAO, IOD and EAO at periods mainly ranging from 3 to 7 years. ENSO and IOD mostly influence wind speed during the winter and autumn months while the remaining two indices affect the summer months at varying periodicity. Linear multiple regression of wind speed as a function of climate indices gave satisfactory performance although it did not capture the relative extremes in wind speeds. Future efforts can focus on the adoption of an objective approach for the identification of wind seasonality in the region (see for instance Cunderlik *et al.*, 2004) and the use of this information for a better prediction of seasonal winds. The methodology presented in the present paper can also be adopted to study the teleconnections and the

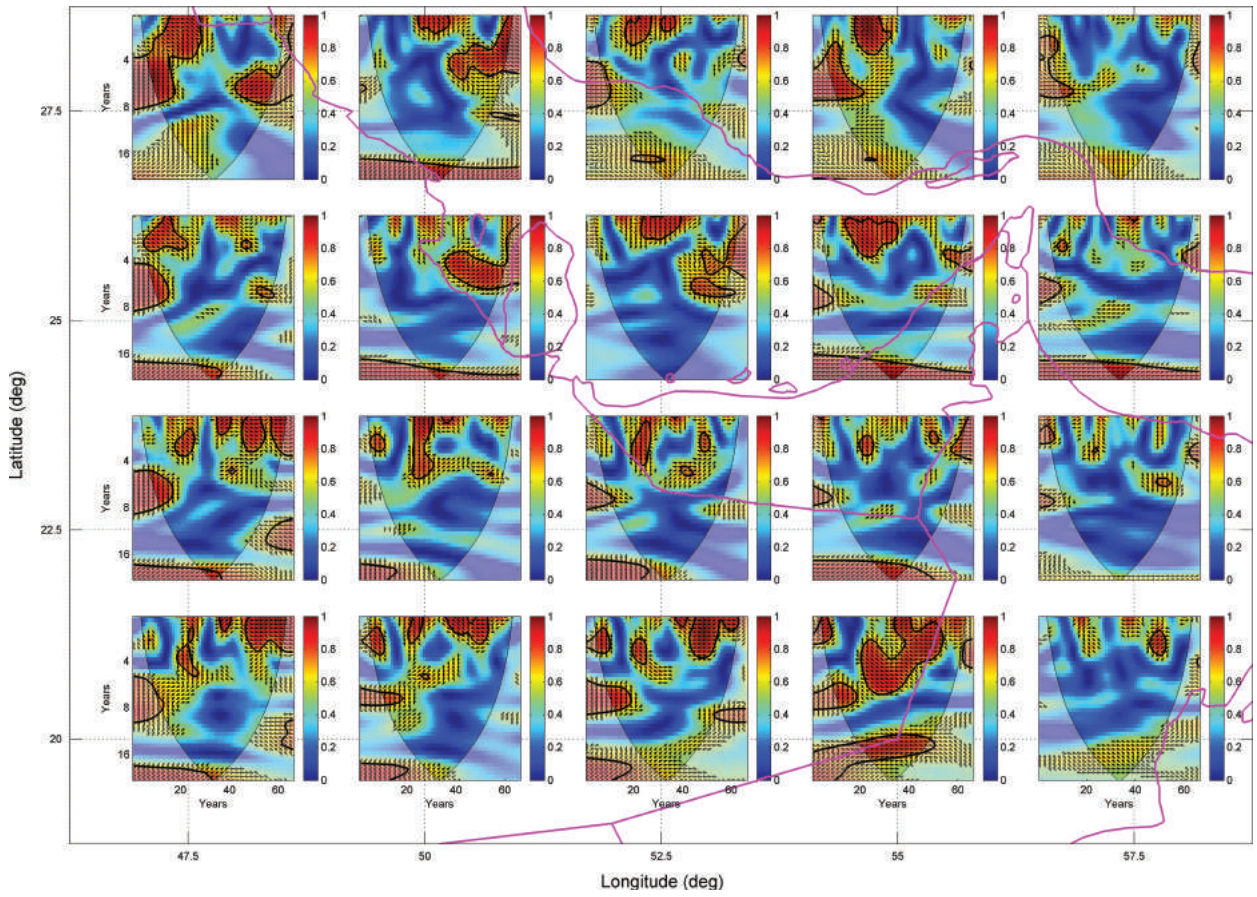

Figure 14. Same as Figure 13 but for the years 1948–2013.

long-term wind speed variability in other regions of the world.

Acknowledgements

The authors wish to thank the National Climate Data Centre (NCDC), National Oceanic and Atmospheric Administration (NOAA) and Climatic Research Unit (CRU) for providing wind and climate indices data. Wavelet computer programs used in this research were adopted from C. Torrence and G.P. Compo (http://paos.colorado.edu/research/wavelets/) and A. Grinsted, J. Moore and S. Jevrejeva (http://noc.ac.uk/using-science/crosswavelet-wavelet-coherence). The authors are grateful to the editor, Dr. Sergey Gulev and the two anonymous reviewers for their comments which greatly helped improve the quality of the paper. The authors would also like to thank Dr. Shaik Basha for his help.

References

Almazroui M. 2012. Temperature variability over saudi arabia and its association with global climate indices. *J. King Abdulaziz Univ. Meteorol. Environ. Arid Land Agric. Sci.* **23**(1): 85–108.

Bannayan M, Sanjani S, Alizadeh A, Lotfabadi SS, Mohamadian A. 2010. Association between climate indices, aridity index, and rainfed crop yield in northeast of Iran. *Field Crop Res.* **118**(2): 105–114, doi: 10.1016/j.fcr.2010.04.011.

Barnston AG, Livezey RE. 1987. Classification, seasonality and persistence of low-frequency atmospheric circulation patterns. *Mon. Weather Rev.* **115**(6): 1083–1126.

Basha G, Ouarda TBMJ, Marpu PR. 2015. Long-term projections of temperature, precipitation and soil moisture using non-stationary oscillation processes over the UAE region. *Int. J. Climatol.* **35**: 4606–4618, doi: 10.1002/joc.4310.

Brook GA, Sheen S-W. 2000. Rainfall in Oman and the United Arab Emirates: cyclicity, influence of the Southern Oscillation, and what the future may hold. *Arab World Geograph.* **3**(2): 78–96.

Chandran A, Basha G, Ouarda TBMJ. 2015. Influence of climate oscillations on temperature and precipitation over the United Arab Emirates. *Int. J. Climatol.* **36**: 225–235, doi: 10.1002/joc.4339.

Charabi Y, Abdul-Wahab SA. 2009. Synoptic aspects of the summer monsoon of southern Oman and its global teleconnections. *J. Geophys. Res.* **114**(D7): D07107, doi: 10.1029/2008JD010234.

Criado-Aldeanueva F, Soto-Navarro FJ. 2013. The mediterranean oscillation teleconnection index: station-based versus principal component paradigms. *Adv. Meteorol.* **2013**: 1–10.

Cullen H, Kaplan A, Arkin P, deMenocal P. 2002. Impact of the North Atlantic Oscillation on Middle Eastern climate and streamflow. *Clim. Chang.* **55**(3): 315–338, doi: 10.1023/A:1020518305517.

Cunderlik JM, Ouarda TBMJ, Bobée B. 2004. On the objective identification of flood seasons. *Water Resour. Res.* **40**(1): W01520, doi: 10.1029/2003WR002295.

Diaz AF, Studzinski CD, Mechoso CR. 1998. Relationships between precipitation anomalies in Uruguay and Southern Brazil and sea surface temperature in the Pacific and Atlantic oceans. *J. Clim.* **11**(2): 251–271, doi: 10.1175/1520-0442(1998)011<0251:RBPAIU>2.0.CO;2.

Diaz HF, Hoerling MP, Eischeid JK. 2001. ENSO variability, teleconnections and climate change. *Int. J. Climatol.* **21**(15): 1845–1862.

Donat M, Peterson T, Brunet M, King A, Almazroui M, Kolli R, Boucherf D, Al-Mulla AY, Nour AY, Aly AA. 2014. Changes in extreme temperature and precipitation in the Arab region: long-term

trends and variability related to ENSO and NAO. *Int. J. Climatol.* **34**(3): 581–592.
El Adlouni S, Ouarda T, Zhang X, Roy R, Bobée B. 2007. Generalized maximum likelihood estimators for the nonstationary generalized extreme value model. *Water Resour. Res.* **43**(3): W03410, doi: 10.1029/2005WR004545.
Fried L. 2014. *Global Wind Statistics 2013*. Global Wind Energy Council (GWEC): Brussels.
Ghasemi AR, Khalili D. 2006. The influence of the Arctic Oscillation on winter temperatures in Iran. *Theor. Appl. Climatol.* **85**(3–4): 149–164, doi: 10.1007/s00704-005-0186-4.
Grinsted A, Moore JC, Jevrejeva S. 2004. Application of the cross wavelet transform and wavelet coherence to geophysical time series. *Nonlinear Process. Geophys.* **11**(5/6): 561–566.
Hamed KH, Rao AR. 1998. A modified Mann-Kendall trend test for autocorrelated data. *J. Hydrol.* **204**(1): 182–196.
Hundecha Y, St-Hilaire A, Ouarda T, El Adlouni S, Gachon P. 2008. A nonstationary extreme value analysis for the assessment of changes in extreme annual wind speed over the Gulf of St. Lawrence, Canada. *J. Appl. Meteorol. Climatol.* **47**(11): 2745–2759.
Hurrell JW. 1995. Decadal trends in the North Atlantic Oscillation: regional temperatures and precipitation. *Science* **269**(5224): 676–679.
Hurrell JW, Deser C. 2010. North Atlantic climate variability: the role of the North Atlantic Oscillation. *J. Mar. Syst.* **79**(3): 231–244.
Jevrejeva S, Moore J, Grinsted A. 2003. Influence of the Arctic Oscillation and El Niño-Southern Oscillation (ENSO) on ice conditions in the Baltic Sea: the wavelet approach. *J. Geophys. Res.* **108**(D21): 4677, doi: 10.1029/2003JD003417.
Joselin Herbert GM, Iniyan S, Sreevalsan E, Rajapandian S. 2007. A review of wind energy technologies. *Renew. Sust. Energ. Rev.* **11**(6): 1117–1145, doi: 10.1016/j.rser.2005.08.004.
Kalnay E, Kanamitsu M, Kistler R, Collins W, Deaven D, Gandin L, Iredell M, Saha S, White G, Woollen J. 1996. The NCEP/NCAR 40-year reanalysis project. *Bull. Am. Meteorol. Soc.* **77**(3): 437–471.
Khaliq M, Ouarda T, Gachon P. 2009a. Identification of temporal trends in annual and seasonal low flows occurring in Canadian rivers: the effect of short-and long-term persistence. *J. Hydrol.* **369**(1): 183–197.
Khaliq M, Ouarda TB, Gachon P, Sushama L, St-Hilaire A. 2009b. Identification of hydrological trends in the presence of serial and cross correlations: a review of selected methods and their application to annual flow regimes of Canadian rivers. *J. Hydrol.* **368**(1): 117–130.
Kiladis GN, Diaz HF. 1989. Global climatic anomalies associated with extremes in the Southern Oscillation. *J. Clim.* **2**(9): 1069–1090.
Kirchner-Bossi N, García-Herrera R, Prieto L, Trigo R. 2014. A long-term perspective of wind power output variability. *Int. J. Climatol.* **35**: 2635–2646, doi: 10.1002/joc.4161.
Lee T, Ouarda T. 2010. Long-term prediction of precipitation and hydrologic extremes with nonstationary oscillation processes. *J. Geophys. Res.* **115**(D13): D13107, doi:10.1029/2009JD012801.
Lee T, Ouarda T, Li J. 2013. An orchestrated climate song from the Pacific and Atlantic Oceans and its implication on climatological processes. *Int. J. Climatol.* **33**(4): 1015–1020, doi: 10.1002/joc.3488.
Li J, Yu R, Zhou T. 2008. Teleconnection between NAO and climate downstream of the Tibetan Plateau. *J. Clim.* **21**(18): 4680–4690.
Mann HB. 1945. Nonparametric tests against trend. *Econometrica* **13**(3): 245–259.
Maraun D, Kurths J. 2004. Cross wavelet analysis: significance testing and pitfalls. *Nonlinear Process. Geophys.* **11**(4): 505–514.
Marcella MP, Eltahir EA. 2008. The hydroclimatology of Kuwait: explaining the variability of rainfall at seasonal and interannual time scales. *J. Hydrometeorol.* **9**(5): 1095–1105.
Nasrallah HA, Balling RC Jr, Selover NJ, Vose RS. 2001. Development of a seasonal forecast model for Kuwait winter precipitation. *J. Arid Environ.* **48**(2): 233–242, doi: 10.1006/jare.2000.0746.
Nasri B, El Adlouni S, Ouarda TB. 2013. Bayesian estimation for GEV-B-Spline model. *Open J. Stat.* **3**(02): 118.
Nazemosadat MJ, Cordery I. 2000. On the relationships between ENSO and autumn rainfall in Iran. *Int. J. Climatol.* **20**(1): 47–61, doi: 10.1002/(SICI)1097-0088(200001)20:1<47::AID-JOC461>3.0.CO;2-P.
Nazemosadat M, Samani N, Barry D. 2006. ENSO forcing on climate change in Iran: precipitation analysis. *Iran. J. Sci. Technol. Trans. B: Eng.* **30**(ECOL-ARTICLE-2007-006): 555–565.
Niranjan Kumar K, Ouarda T. 2014. Precipitation variability over UAE and global SST teleconnections. *J. Geophys. Res.: Atmos.* **119**(17): 10,313–10,322.
Oliver J. 2012. *El Nino Southern Oscillation, Climate Indices and Their Relationship With Wind Speed in the Texas Panhandle*. Research Americas: Broomfield, CO.
Ouachani R, Bargaoui Z, Ouarda T. 2013. Power of teleconnection patterns on precipitation and streamflow variability of upper Medjerda Basin. *Int. J. Climatol.* **33**(1): 58–76, doi: 10.1002/joc.3407.
Ouarda T, El-Adlouni S. 2011. Bayesian nonstationary frequency analysis of hydrological variables 1. *J. Am. Water Resour. Assoc.* **47**(3): 496–505.
Ouarda T, Charron C, Niranjan Kumar K, Marpu P, Ghedira H, Molini A, Khayal I. 2014. Evolution of the rainfall regime in the United Arab Emirates. *J. Hydrol.* **514**: 258–270.
Ouarda T, Charron C, Shin J-Y, Marpu P, Al-Mandoos A, Al-Tamimi M, Ghedira H, Al Hosary T. 2015. Probability distributions of wind speed in the UAE. *Energy Convers. Manag.* **93**: 414–434.
Perrone T. 1979. Winter Shamal in the Persian Gulf, Naval Environmental Prediction Research Facility. Technical Report No. 79-06, Naval Environmental Prediction Research Facility: Monterey, 188 pp.
Romero C, Baigorria G, Stroosnijder L. 2007. Changes of erosive rainfall for El Niño and La Niña years in the northern Andean highlands of Peru. *Clim. Chang.* **85**(3–4): 343–356, doi: 10.1007/s10584-007-9301-0.
Ropelewski CF, Halpert MS. 1986. North American precipitation and temperature patterns associated with the El Niño/Southern Oscillation (ENSO). *Mon. Weather Rev.* **114**(12): 2352–2362.
Saji N, Yamagata T. 2003. Possible impacts of Indian Ocean dipole mode events on global climate. *Clim. Res.* **25**(2): 151–169.
Scaife A, Arribas A, Blockley E, Brookshaw A, Clark R, Dunstone N, Eade R, Fereday D, Folland C, Gordon M. 2014. Skillful long-range prediction of European and North American winters. *Geophys. Res. Lett.* **41**(7): 2514–2519.
Seidou O, Ouarda TB. 2007. Recursion-based multiple change-point detection in multiple linear regression and application to river streamflows. *Water Resour. Res.* **43**(7): W07404, doi: 10.1029/2006WR005021.
Smith DM, Scaife AA, Eade R, Knight JR. 2014. Seasonal to decadal prediction of the winter North Atlantic Oscillation: emerging capability and future prospects. *Q. J. R. Meteorol. Soc.*, doi: 10.1002/qj.2479.
Tabari H, Hosseinzadeh Talaee P, Willems P. 2014. Links between Arctic Oscillation (AO) and inter-annual variability of Iranian evapotranspiration. *Quat. Int.* **345**(0): 148–157, doi: 10.1016/j.quaint.2014.02.011.
Torrence C, Compo GP. 1998. A practical guide to wavelet analysis. *Bull. Am. Meteorol. Soc.* **79**(1): 61–78.
Torrence C, Webster PJ. 1999. Interdecadal changes in the ENSO-monsoon system. *J. Clim.* **12**(8): 2679–2690.
Trigo RM, Pozo-Vázquez D, Osborn TJ, Castro-Díez Y, Gámiz-Fortis S, Esteban-Parra MJ. 2004. North Atlantic oscillation influence on precipitation, river flow and water resources in the Iberian Peninsula. *Int. J. Climatol.* **24**(8): 925–944, doi: 10.1002/joc.1048.
Zhang Y, Wallace JM, Battisti DS. 1997. ENSO-like interdecadal variability: 1900–93. *J. Clim.* **10**(5): 1004–1020.
Zhang Q, Xu C-y, Jiang T, Wu Y. 2007. Possible influence of ENSO on annual maximum streamflow of the Yangtze River, China. *J. Hydrol.* **333**(2–4): 265–274, doi: 10.1016/j.jhydrol.2006.08.010.

